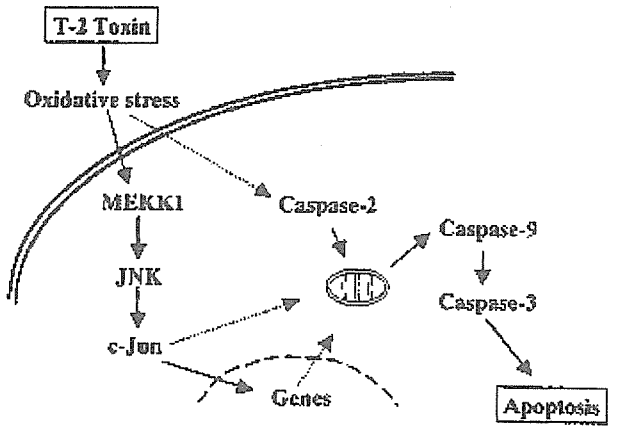

Fig. 18. Hypothesis of mechanisms involved in T-2 toxin-induced apoptosis in rat fetal brain. (Sehata *et al.*, Exp Toxic Pathol. 57: 15–28. 2005 (modified)).

2 toxin-treated fetal brain, is induced by reactive oxygen species, and caspase-2 plays a critical and singular role in the control of apoptosis[117]. Therefore, the increased gene expression of caspase-2 may also indicate the involvement of caspase-2 in T-2 toxin-induced apoptosis in the fetal brain.

Sehata *et al.* (2004) have also reported the decreased expression of many metabolism-related genes, especially lipid metabolism- and drug metabolizing enzyme-related genes. In addition, decreased expression of mitochondria-related genes, such as mitochondrial NADH-dehydrogenase and cytochrome oxidase, and of the mitochondrial genome, has also been detected in the fetal brain, suggesting a dysfunction of the mitochondria as a result of the T-2 toxin treatment.

Judging from these data, it is concluded that T-2 toxin induces oxidative stress, followed by activation of the MAPK pathway, finally resulting in apoptosis in the fetal rat brain and that the *c-jun* gene plays an important role in the induction of apoptosis (Fig. 18). In addition, there is a possibility that the TNF-α receptor pathway may also be involved in the mechanisms of T-2 toxin-induced apoptosis in the rat fetal brain.

Conclusion

T-2 toxin induces apoptosis in hematopoietic, lymphoid and gastrointestinal tissues, dorsal skin and fetal tissues such as the central nervous and skeletal systems, and the development of T-2 toxin-induced apoptosis differs among tissues. T-2 toxin-induced apoptosis is not absolutely related to the suppression of proliferating activity of component cells by T-2 toxin, and T-2 toxin-induced apoptosis involves tissue-specific as well as common mechanisms. New research techniques such as microarray analysis will contribute to progress in our understanding of the mechanisms of apoptosis.

References

1. Desjardins AE, Hohn TM, and McCormick SP. Trichothecene biosynthesis in *Fusarium* species: chemistry, genetics, and significance. Microbiol Rev. **57**: 595–604. 1993.
2. Nelson PE, Dignani MC, and Anaissie EJ. Taxonomy, biology, and clinical aspects of *Fusarium* species. Clin Microbiol Rev. 7: 479–504. 1994.
3. Yagen B and Bialer M. Metabolism and pharmacokinetics of T-2 toxin and related trichothecenes. Drug Metab Rev. **25**: 281–323. 1993.
4. Bamburg JR, Riggs NV, and Strong FM. The structures of toxins from two strains of Fusarium tricinctum. Tetrahedron. **24**: 3329–3336. 1968.
5. Joffe A. Toxicity of *Fusarium poae* and *F. sporotrichiodes* and its relation to alimentary aleukia. In: Mycotoxins. IFH Purchase (ed). Els. Scient. Publish. Comp., Amsterdam. 229–262. 1974.
6. Mirocha CJ. Effect of trichothecene mycotoxins on farm animals. In: Trichothecenes: Chemical, Biological and Toxicological Aspects. Y Ueno (ed). Kodansha Ltd., Tokyo. 177–194. 1983.
7. Ueno Y, Ishii K, Sakai K, Kanaeda S, and Tsunoda H. Toxicological approaches to the metabolites of *Fusaria*. IV. Microbial survey on "bean-hulls poisoning of horses" with the isolation of toxic trichothecenes, neosolaniol and T-2 toxin of *Fusarium solani* M-1-1. Jpn J Exp Med. **42**: 187–203. 1972.
8. Eriksen GS and Pettersson H. Toxicological evaluation of trichothecenes in animal feed. Animal Feed Science and Technology. **114**: 205–239. 2004.
9. Stanford GK, Hood RD, and Hayes AW. Effect of prenatal administration of T-2 toxin to mice. Res Commun Chem Pathol Pharmacol. **10**: 743–746. 1975.
10. Williams PP. Effects of T-2 mycotoxin on gastrointestinal tissues: a review of *in vivo* and *in vitro* models. Arch Environ Contam Toxicol. **18**: 374–387. 1989.
11. IARC. IARC monographs on the evaluation of the carcinogenic risk of chemicals to humans series. In: IARC Monographs on the Evaluation of the Carcinogenic Risk of Chemicals to Humans. Lyon, France. 467–488. 1993.
12. Sharma RP. Immunotoxicity of mycotoxins. J Dairy Sci. **76**: 892–897. 1993.
13. Magnuson BA, Schiefer HB, Hancock DS, and Bhatti AR. Cardiovascular effects of mycotoxin T-2 after topical application in rats. Can J Physiol Pharmacol. **65**: 799–802. 1987.
14. Lutsky I and Mor N. Experimental alimentary toxic aleukia in cats. Lab Anim Sci. **31**: 43–47. 1981.
15. Matsumoto H, Ito T, and Ueno Y. Toxicological approaches to the metabolites of *Fusaria*. XII. Fate and distribution of T-2 toxin in mice. Jpn J Exp Med. **48**: 393–399. 1978.
16. Corley RA, Swanson SP, Gullo GJ, Johnson L, Beasley VR, and Buck WB. Disposition of T-2 toxin, a trichothecene mycotoxin, in intravascularly dosed swine. J Agric Food Chem. **34**: 868–875. 1986.
17. Beasley VR, Swanson SP, Corley RA, Buck WB, Koritz GD, and Burmeister HR. Pharmacokinetics of the trichothecene mycotoxin, T-2 toxin, in swine and cattle. Toxicon. **24**: 13–23. 1986.
18. Coddington KA, Swanson SP, Hassan AS, and Buck WB.

Enterohepatic circulation of T-2 toxin metabolites in the rat. Drug Metab Dispos. **17**: 600–605. 1989.
19. Shifrin VI and Anderson P. Trichothecene mycotoxins trigger a ribotoxic stress response that activates c-jun N-terminal kinase and p38 mitogen-activated protein kinase and induces apoptosis. J Biol Chem. **274**: 13985–13992. 1999.
20. Bennet JW and Klich M. Mycotoxins. Clin Microbiol Rev. **16**: 497–516. 2003.
21. Thompson WL and Wannemacher RW Jr. *In vivo* effects of T-2 mycotoxin on synthesis of protein and DNA in rat tissues. Toxicol Appl Pharmacol. **105**: 483–491. 1990.
22. Chang IM and Mar WC. Effect of T-2 toxin on lipid peroxidation in rats: elevation of conjugated diene formation. Toxicol Letts. **40**: 275–280. 1988.
23. Eriksen GS, Pettersson H, and Lund H. Comparative cytotoxicity of deoxynivalenol, nivalenol, their acetylated derivatives and de-epoxy metabolites. Food Chem Toxicol. **42**: 619–624. 2004.
24. Quiroga MA, Itagaki S, and Doi K. Early ultrastructural changes of thymocytes in T-2 toxicated mice. J Toxicol Pathol. **6**: 109–112. 1993.
25. Shinozuka J, Li G, Kiatipattanasakul W, Uetsuka K, Nakayama H, and Doi K. T-2 toxin-induced apoptosis in lymphoid organs of mice. Exp Toxicol Pathol. **49**: 387–392. 1997.
26. Gavrieli Y, Sherman Y, and Ben-Sasson SA. Identification of programmed cell death in situ via specific labeling of nuclear DNA fragmentation. J Cell Biol. **119**: 493–501. 1992.
27. Shinozuka J, Suzuki M, Noguchi N, Sugimoto T, Uetsuka K, Nakayama H, and Doi K. T-2 toxin-induced apoptosis in hematopoietic tissues of mice. Toxicol Pathol. **26**: 674–681. 1998.
28. Hayes MA and Schiefer HB. Comparative toxicity of dietary T-2 toxin in rats and mice. J. Appl. Toxicol. **2**: 207–212. 1982.
29. Smith BJ, Holladay SD, and Blaylock BL. Hematopoietic alterations after exposure to T-2 mycotoxin. Toxicon. **32**: 1115–1123. 1994.
30. Seifert MF and Marks SC Jr. The regulation of hemopoiesis in the spleen. Experimentia. **41**: 192–199. 1985.
31. Shinozuka J and Doi K. T-2 toxin-induced apoptosis in the mouse lymphoid and hematopoietic tissues. Mycotoxins. **53**: 129–139. 2003.
32. Rosenstein Y and Lafarge-Frayssinet C. Inhibitory effect of Fusarium T2-toxin on lymphoid DNA and protein synthesis. Toxicol Appl Pharmacol. **70**: 283–288. 1983.
33. Velazco V, Faifer GC, and Godoy HM. Differential effects of T-2 toxin on bone marrow and spleen erythropoiesis in mice. Food Chem Toxicol. **34**: 371–375. 1996.
34. Segal R, Milo-Goldzweig I, Joffe AZ, and Yagen B. Trichothecene-induced hemolysis. I. The hemolytic activity of T-2 toxin. Toxicol Appl Pharmacol. **70**: 343–349. 1983.
35. DeLoach JR, Gyongyossy-Issa MI, and Khachatouriants GG. Species-specific hemolysis of erythrocytes by T-2 toxin. Toxicol Appl Pharmacol. **97**: 107–112. 1989.
36. Gyongyossy-Issa MI and Khachatourians GG. Interaction of T-2 toxin with murine lymphocytes. Biochem Biophys Acta. **803**: 197–202. 1984.
37. Nagata T, Suzuki H, Ishigami N, Shinozuka J, Uetsuka K, Nakayama H, and Doi K. Development of apoptosis and changes in lymphocyte subsets in thymus, mesenteric lymph nodes and Peyer's patches of mice orally inoculated with T-2 toxin. Exp Toxicol Pathol. **53**: 309–315. 2001.
38. Shinozuka J, Li G, Uetsuka K, Nakayama H, and Doi K. Process of the development of T-2 toxin-induced apoptosis in the lymphoid organs of mice. Exp Anim. **46**: 117–126. 1997b.
39. Smith BJ, Holladay SD, and Blaylock BL. Hematopoietic alterations after exposure to T-2 mycotoxins. Toxicon. **32**: 1115–1123. 1994.
40. Islam Z, Nagase M, and Yoshizawa T. T-2 toxin induces thymic apoptosis in vivo in mice. Toxicol Appl Pharmacol. **148**: 205–214. 1998.
41. Holladay SD, Smith BJ, and Luster MI. B lymphocyte precursor cells represent sensitive targets of T2 mycotoxin exposure. Toxicol Appl Pharmacol. **131**: 309–315. 1995.
42. Shortman K, Egerton M, Spangrude GJ, and Scollay R. The generation and fate of thymocytes. Semin Immunol. **2**: 3–12. 1990.
43. Holladay SD, Blaylock BL, Comment CE, Heindel JJ, and Luster MI. Fetal thymic atrophy after exposure to T-2 toxin: selectivity for lymphoid progenitor cells. Toxicol Appl Pharmacol. **121**: 8–14. 1993.
44. Butcher EC, Rouse RV, Coffman RL, Nottenburg CN, Hardy RR, and Weissman IL. Surface phenotype of Peyer's patch germinal center cells: implications for the role of germinal centers in B cell differentiation. J Immunol. **129**: 2698–2707. 1982.
45. Harriman GR, Kunimoto DY, Elliott JF, Paetkau V, and Strober W. The role of IL-5 in IgA B cell differentiation. J Immunol. **140**: 3033–3039. 1988.
46. Weinstein PD and Cebra JJ. The preference for switching to IgA expression by Peyer's patch germinal center B cells is likely due to the intrinsic influence of their microenvironment. J Immunol. **147**: 4126–4135. 1991.
47. Shinozuka J, Tsutsui S, Ishigami N, Ueno-Yamanouchi A, Nakayama H, and Doi K. Development of apoptosis and changes in apoptosis-related genes expression in the mouse thymus following T-2 toxin-inoculation. J Toxicol Pathol. **12**: 77–81. 1999.
48. Alam MM, Nagase M, Yoshizawa T, and Sakato N. Thymocyte apoptosis by T-2 toxin in vivo in mice is independent of Fas/Fas ligand system. Biosci Biotechnol Biochem. **64**: 210–213. 2000.
49. Verma IM, Mitchell RL, Kruijer W, Beveren CV, Zokas L, Hunter T and Cooper JA. Proto-oncogene c-fos: induction and regulation during growth and differentiation. Cancer Cells. **3**: 275–287. 1985.
50. Lau LF and Nathans D. Expression of a set of growth-related immediate early genes in BALB/c 3T3 cells: coordinate regulation with *c-fos* or *c-myc*. Proc Natl Acad Sci. **84**: 1182–1186. 1987.
51. Smeyne RJ, Vendrell M, Hayward M, Baker SJ, Miao GG, Schilling K, Robertson LM, Curran T, and Morgan JI. Continuous c-fos expression precedes programmed cell death *in vivo*. Nature. **363**: 166–169. 1993.
52. Marti A, Jehn B, Costello E, Keon N, Ke G, Martin F, and Jaggi R. Protein kinase A and AP-1 (c-Fos/JunD) are induced during apoptosis of mouse mammary epithelial cells. Oncogene. **9**: 1213–1223. 1994.
53. Mils V, Piette J, Barette C, Veyrune J, Tesniere A, Escot C, Guilhou JJ, and Basset-Seguin N. The proto-oncogene *c-fos*

increases the sensitivity of keratinocytes to apoptosis. Oncogene. **14**: 1555–1561. 1997.
54. Colotta F, Polentarutti N, Sironi M, and Mantovani A. Expression and involvement of *c-fos* and *c-jun* protooncogenes in programmed cell death induced by growth factor deprivation in lymphoid cell lines. J Biol Chem. **267**: 18278–18283. 1992.
55. Buttyan R, Zakeri Z, Lockshin R, and Wolgemuth D. Cascade induction of *c-fos*, *c-myc*, and *heat shock 70K* transcripts during repression of the rat ventral prostate gland. Mol Endocrinol. **2**: 650–657. 1988.
56. Preston GA, Lyon TT, Yin Y, Lang JE, Solomon G, Annab L, Srinivasan DG, Alcorta DA, and Barrett JC. Induction of apoptosis by c-Fos protein. Mol Cell Biol. **16**: 211–218. 1996.
57. Shinozuka J, Suzuki H, Tsutsui S, Nakayama H, and Doi K. T-2 toxin-induced apoptosis and *c-fos* mRNA expression in ConA-stimulated mouse thymocyte primary cultures. J Toxicol Pathol. **14**: 247–251. 2001.
58. Morgan JI and Curran T. Calcium as a modulator of the immediate-early gene cascade in neurons. Cell Calcium. **9**: 303–311. 1988.
59. Maki A, Berezesky IK, Fargnoli J, Holbrook NJ, and Trump BF. Role of $[Ca^{2+}]_i$ in induction of c-fos, c-jun and c-myc mRNA in rat PTE after oxidative stress. FASEB J. **6**: 919–924. 1992.
60. Yamamoto N, Smith MW, Maki A, Berezesky IK, and Trump BF. Role of cytosolic Ca^{2+} and protein kinases in the induction of the *hsp70* gene. Kidney Int. **45**: 1093–1104. 1994.
61. Yoshino N, Takizawa M, Akiba H, Okumura H, Tashiro F, Honda M, and Ueno Y. Transient elevation of intracellular calcium ion levels as an early event in T-2 toxin-induced apoptosis in human promyelotic cell line HL-60. Nat Toxins. **4**: 234–241. 1996.
62. Cohen DR and Curran T. The structure and function of the fos proto-oncogene. Crit Rev Oncog. **1**: 65–88. 1989.
63. Nagase M, Alam MM, Tsushima A, Yoshizawa T, and Sakato N. Apoptosis induction by T-2 toxin: activation of caspase-9, caspase-3, and DFF-40/CAD through cytosolic release of cytochrome c in HL-60 cells. Biosci Biotechnol Biochem. **65**: 1741–1747. 2001.
64. Quiroga MA, Risso MA, Perfumo CJ, Idiart JR, Ohtsuka R, and Doi K. Sequence of and regional difference in apoptotic index in the mouse gastrointestinal mucous epithelia after T-2 toxin inoculation. J Toxicol Pathol. **13**: 193–196. 2000.
65. Li G, Shinozuka J, Uetsuka K, Nakayama H, and Doi K. T-2 toxin-induced apoptosis in intestinal crypt epithelial cells oh mice. Exp Toxicol Pathol. **49**: 447–450. 1997.
66. Li G, Shinozuka J, Uetsuka K, Nakayama H, and Doi K. T-2 toxin-induced apoptosis in Peyer's patches of mice. J Toxicol Pathol. **10**: 59–61. 1997.
67. Kemppainen BW, Riley RT, and Pace JG. Penetration of [^{3}H] T-2 toxin through excised human and guinea-pig skin during exposure to [^{3}H] T-2 toxin adsorbed to corn dust. Food Chem Toxic. **22**: 893–896. 1984.
68. Bunner BL, Wannemacher RW Jr, Dinterman RE, and Broski FH. Cutaneous absorption and decontamination of [^{3}H] T-2 toxin in rat model. J Toxicol Environ Health. **26**: 413–423. 1989.
69. Solberg VB, Broski FH, Dinterman RE, and George DT. Penetration of [^{3}H] T-2 mycotoxin through abraded and intact skin and methods to decontaminate [^{3}H] T-2 mycotoxin from abrasions. Toxicon. **28**: 803–811. 1990.
70. Yarom R, Bergmann F, and Yagen B. Cutaneous injury by topical T-2 toxin: involvement of microvessels and mast cells. Toxicon. **25**: 167–174. 1987.
71. Bhavanishankar TN, Ramesh HP, and Shantha T. Dermal toxicity of Fusarium toxins in combinations. Arch Toxicol. **61**: 241–244. 1988.
72. Schiefer HB and Hancock DS. Systemic effects of topical application of T-2 toxin in mice. Toxicol Appl Pharmacol. **76**: 464–472. 1984.
73. Blaylock BL, Kouchi Y, Comment CE, Pollock PL, and Luster MI. Topical application of T-2 toxin inhibits the contact hypersensitivity response in BALB/c mice. J Immunol. **150**: 5135–5143. 1993.
74. Iwamoto S, Nakayama H, and Doi K. Morphological and morphometrical study on the dorsal skin of Wistar and WBN/ILA-Ht rats in their developing stage. Evaluation of the proliferation and apoptotic processes. Histol Histopathol. **13**: 981–988. 1998.
75. Albarenque SM, Shinozuka J, Iwamoto S, Nakayama H, and Doi K. T-2 toxin-induced acute skin lesions in Wistar-derived hypotrichotic WBN/ILA-*Ht* rats. Histol Histopathol. **14**: 337–342. 1999.
76. Albarenque SM, Suzuki K, Shinozuka J, Nakayama H, and Doi K. Kinetics of apoptosis-related genes mRNAs expression in the dorsal skin of hypotrichotic WBN/ILA-*Ht* rats after topical application of T-2 toxin. Exp Toxicol Pathol. **52**: 553–556. 2001.
77. Mils V, Piette J, Barette C, Veyrune J, Tesniere A, Escot C, Guilhou JJ, and Basset-Seguin N. The proto-oncogene c-fos increases the sensitivity of keratinocytes to apoptosis. Oncogene. **14**: 1555–1561. 1997.
78. Shifrin V and Anderson P. Trichothecene mycotoxins trigger a ribotoxic stress response that activates c-Jun N-terminal kinase and p38 mitogen-activated protein kinase and induces apoptosis. J Biol Chem. **274**: 13985–13992. 1999.
79. Iordanov MS and Magun BE. Loss of cellular K^+ mimics ribotoxic stress. Inhibition of protein synthesis and activation of the stress kinases SEK1/MKK4, stress-activated protein kinase/c-Jun NH2-terminal kinase 1, and p38/HOG1 by palytoxin. J Biol Chem. **273**: 3528–3534. 1998.
80. Albarenque SM, Shinozuka J, Suzuki K, Nakayama H, and Doi K. Kinetics and distribution of transforming growth factor (TGF)-β1 mRNA in the dorsal skin of hypotrichotic WBN/ILA-*Ht* rats following topical application of T-2 toxin. Exp Toxicol Pathol. **52**: 297–301. 2000.
81. Benassi L, Ottani D, Fantini F, Marconi A, Chiodino C, Giannetti A, and Pincelli C. 1, 25-Dihydroxyvitamin D3, transforming growth factor (TGF)-β1, calcium, and ultraviolet B radiation induce apoptosis in cultured human keratinocytes. J Invest Dermatol. **109**: 276–282. 1997.
82. Gruber BL, Marchese MJ, and Kew RR. Transforming growth factor-β1 mediates mast cell chemotaxis. J Immunol. **152**: 5860–5867. 1994.
83. Kane CJ, Hebda PA, Mansbridge JN, and Hanawalt PC. Direct evidence for spatial and temporal regulation of transforming growth factor-β1 expression during cutaneous wound healing. J Cell Physiol. **148**: 157–173. 1991.
84. Roberts AB, McCune BK, and Sporn MB. TGF-beta: regulation of extracellular matrix. Kidney Int. **41**: 557–559.

1992.
85. Albarenque SM, Suzuki K, Nakayama H, and Doi K. Kinetics of cytokines mRNAs expression in the dorsal skin of WBN/ILA-*Ht* rats following topical application of T-2 toxin. Exp Toxicol Pathol. **53**: 271–274. 2001.
86. Köck A, Urbanski A, and Luger T. mRNA expression and release of tumor necrosis factor-α by human epidermal cells. J Invest Dermatol. **92**: 462A. 1989.
87. Schwarz A, Bhardwaj R, Aragane Y, Mahnke K, Riemann H, Metze D, Luger TA, and Schwarz T. Ultraviolet-B-induced apoptosis of keratinocytes: evidence for partial involvement of tumor necrosis factor-alpha in the formation of sunburn cells. J Invest Dermatol. **104**: 922–927. 1995.
88. Meng X, Sawamura D, Baba T, Ina S, Ita K, Tamai K, Hanada K, and Hashimoto I. Transgenic TNF-α causes apoptosis in epidermal keratinocytes after subcutaneous injection of TNF-α DNA plasmid. J Invest Dermatol. **113**: 856–857. 1999.
89. Zhuang L, Wang B, Shinder GA, Shivji GM, Mak TW, and Sauder DN. TNF receptor p55 plays a pivotal role in murine keratinocyte apoptosis induced by ultraviolet B irradiation. J Immunol **162**: 1440–1447. 1999.
90. Barker JN, Mitra RS, Griffiths CE, Dixit VM, and Nickoloff BJ. Keratinocytes as indicators of inflammation. Lancet. **337**: 211–214. 1991.
91. Griffiths CE, Barker JN, Kunkel S, and Nickoloff BJ. Modulation of leucocyte adhesion molecules, a T-cell chemotaxin (IL-8) and a regulatory cytokine (TNF-α) in allergic contact dermatitis (rhus dermatitis). Br J Dermatol. **124**: 519–526. 1991.
92. Nickoloff BJ and Naidu Y. Perturbation of epidermal barrier function correlates with inhibition of cytokine cascade in human skin. J Am Acad Dermatol. **30**: 535–546.1994.
93. Albarenque SM and Doi K. T-2 toxin-induced apoptosis in rat keratinocyte primary cultures. Exp Mol Pathol. **78**: 144–149. 2005.
94. Lafarge-Frayssinet C, Chakor K, Lafont P, and Frayssinet C. Transplacentral transfer of T2-toxin: pathological effect. J Environ Pathol Toxicol Oncol. **10**: 64–68. 1990.
95. Rousseaux CG and Schiefer HB. Maternal toxicity, embryolethality and abnormal fetal development in CD-1 mice following one oral dose of T-2 toxin. J Appl Toxicol. 7: 281–288. 1987.
96. Sehata S, Teranishi M, Atsumi F, Uetsuka K, Nakayama H, and Doi K. T-2 toxin-induced morphological changes in pregnant rats. J Toxicol Pathol. **16**: 59–65. 2003.
97. Sehata S, Kiyosawa N, Makino T, Atsumi F, Ito K, Yamato T, Teranishi M, Baba Y, Uetsuka K, Nakayama H, and Doi K. Morphological and microarray analysis of T-2 toxin-induced fetal brain lesion. Food Chem Toxicol. **42**: 1727–1736. 2004.
98. Stanford GK, Hood RD, and Hayes AW. Effect of prenatal administration of T-2 toxin to mice. Res Commun Chem Pathol Pharmacol. **10**: 743–746. 1975.
99. Hood RD, Kuczuk MH, and Szczech GM. Effects in mice of simultaneous prenatal exposure to ochratoxin A and T-2 toxin. Teratology. **17**: 25–29. 1978.
100. Khera KS. Maternal toxicity—a possible factor in fetal malformations in mice. Teratology. **29**: 411–416. 1984.
101. Ishigami N, Shinozuka J, Katayama K, Nakayama H, and Doi K. Apoptosis in mouse fetuses from dams exposed to T-2 toxin at different days of gestation. Exp Toxicol Pathol. **52**: 493–501. 2001.
102. Ishigami N, Shinozuka J, Katayama K, Uetsuka K, Nakayama H, and Doi K. Apoptosis in the developing mouse embryos from T-2 toxin-inoculated dams. Histol Histopathol. **14**: 729–733. 1999.
103. Kniesel U, Risau W, and Wolburg H. Development of blood-brain barrier tight junctions in the rat cortex. Brain Res Dev Brain Res. **23**: 229–240. 1996.
104. Ciriolo MR, De Martino A, Lafavia E, Rossi L, Carri MT, and Rotilio G. Cu,Zn-superoxide dismutase-dependent apoptosis induced by nitric oxide in neuronal cells. J Biol Chem. **275**: 5065–5072. 2000.
105. Garrido C, Gurbuxani S, Ravagnan L, and Kroemer G. Heat shock proteins: endogenous modulators of apoptotic cell death. Biochem. Biophys Res Commun. **286**: 433–442. 2001.
106. Hidalgo J, Aschner M, Zatta P, and Vasak M. Roles of the metallothionein family of proteins in the central nervous system. Brain Res Bull. **55**: 133–145. 2001.
107. Ryter SW, Otterbein LE, Morse D, and Choi AM. Heme oxygenase/carbon monoxide signaling pathways: regulation and functional significance. Mol Cell Biochem. **234–235**: 249–263. 2002.
108. Sastry PS and Rao KS. Apoptosis and the nervous system. J Neurochem. **74**: 1–20. 2000.
109. Sehata S, Kiyosawa N, Atsumi F, Ito K, Yamato T, Teranishi M, Uetsuka K, Nakayama H, and Doi K. Microarray analysis of T-2 toxin-induced liver, placenta and fetal liver lesions in pregnant rats. Exp Toxicol Pathol. **57**: 15–28. 2005.
110. Jarpe MB, Widmann C, Knall C, Schlesinger TK, Gibson S, Yujiri T, Fanger GR, Gelfand EW, and Johnson GL. Anti-apoptotic versus pro-apoptotic signal transduction: checkpoints and stop signs along the road to death. Oncogene. **17**: 1475–1482. 1998.
111. Boldt S, Weidle UH, and Kolch W. The kinase domain of MEKK1 induces apoptosis by dysregulation of MAP kinase pathways. Exp Cell Res. **283**: 80–90. 2003.
112. Ham J, Eilers A, Whitfield J, Neame SJ, and Shah B. c-Jun and the transcriptional control of neuronal apoptosis. Biochem Pharmacol. **60**: 1015–1021. 2000.
113. Shifrin VI and Anderson P. Trichothecene mycotoxins trigger a ribotoxic stress response that activates c-jun N-terminal kinase and p38 mitogen-activated protein kinase and induces apoptosis. J Biol Chem. **274**: 13985–13992. 1999.
114. Yang GH, Jarvis BB, Chung YJ, and Pestka JJ. Apoptosis induction by the satratoxins and other trichothecene mycotoxins: relationship to ERK, p38 MAPK, and SAPK/JNK activation. Toxicol Appl Pharmacol. **164**: 149–160. 2000.
115. Bond M, Murphy G, Bennett MR, Newby AC, and Baker AH. Tissue inhibitor of metalloproteinase-3 induces a Fas-associated death domain-dependent type II apoptotic pathway. J Biol Chem. **277**: 13787–13795. 2002.
116. Cohen GM. Caspases: the executioners of apoptosis. Biochem J. **326**: 1–16. 1997.
117. Annunziato L, Amoroso S, Pannaccione A, Cataldi M, Pignataro G, D'Alessio A, Sirabella R, Secondo A, Sibaud L, and Di Renzo GF. Apoptosis induced in neuronal cells by oxidative stress: role played by caspases and intracellular calcium ions. Toxicol Lett. **139**: 125–133. 2003.

Histol Histopathol (2006) 21: 257-263

http://www.hh.um.es

Histology and Histopathology
Cellular and Molecular Biology

Histopathological changes in the brain of mouse fetuses by etoposide-administration

C. Nam, G.H. Woo, K. Uetsuka, H. Nakayama and K. Doi
Department of Veterinary Pathology, Graduate School of Agricultural and Life Sciences,
The University of Tokyo, Bunkyo-ku, Tokyo, Japan

Summary. Etoposide (VP-16), a topoisomerase II inhibitor, is an anti-tumor agent which is also known to show embryotoxicity, and teratogenicity when administered to pregnant rodents. We examined VP-16-induced histopathological changes in the brain of mouse fetuses. Pregnant mice were intraperitoneally injected with VP-16 (4 mg/kg) on day 12 of gestation (GD 12), and fetuses were collected from 1 to 48 hours after treatment (HAT). Mitotic neuroepithelial cells in the telencephalic wall prominently decreased at 2 HAT, and were hardly observed at 4 HAT. The number of pyknotic neuroepithelial cells in the fetal brain began to increase at 4 HAT, and became prominent from 8 to 24 HAT. These pyknotic cells were also positively stained by TUNEL method, which can detect fragmented DNA, and showed ultrastructural characteristics of apoptosis. Additionally, these cells were also positive for cleaved caspase-3, an essential executioner of apoptosis. This indicated that excessive neuroepithelial cell apoptosis was induced in the brain of mouse fetuses following VP-16 treatment on GD 12.

Key words: Apoptosis, Brain, Etoposide, Fetus, Mouse

Introduction

Epotoside (VP-16) is a semisynthetic derivative of podophyllotoxin, which is extracted from a plant *Podophyllum peltatum* and has an antitumor activity (Sieber et al., 1978). VP-16 is widely used as an anticancer chemotherapeutic agent for small cell lung cancer, testicular cancers and lymphomas (Hande, 1998). VP-16, a topoisomerase II inhibitor, impairs DNA synthesis by forming complexes with the cleaved DNA and prevents relegation of the double-strand breaks in the replicating cells (Chen and Liu, 1994). On the other hand, VP-16 is embryocidal and teratogenic in rats and mice. For example, a single intraperitoneal injection of VP-16 to pregnant mice on day 6, 7, or 8 of gestation (GD 6, 7 or 8) caused embryotoxicity, cranial abnormality, and major skeletal malformation (Sieber et al., 1978).

However, details of histopathological changes were not investigated in the brain of fetuses following VP-16 administration to their dams. Therefore, we carried out detailed histopathological examination on the fetal brain obtained from pregnant mice which were treated with VP-16 on GD 12.

Offprint request to: Dr. Chunja Nam, Department of Veterinary Pathology, Graduate School of Agricultural and Life Sciences, The University of Tokyo, 1-1-1 Yayoi, Bunkyo-ku, Tokyo 113-8657, Japan. e-mail: vet0215@yahoo.co.kr

Materials and methods

Animals and treatments

Eight-week-old pregnant ICR (Crj:CD-1) mice were obtained from Charles River Japan Co., Yokohama, Japan. Mice were kept using an isolator caging system (Niki Shoji Co., Tokyo) under controlled conditions (23±2°C with 55±5% humidity and a 14-hr light/10-hr dark cycle) and fed commercial pellets (MF, Oriental Yeast Co., Ltd., Tokyo) and tap water ad libitum. VP-16 (Sigma, St. Louis, MO) was first dissolved in 1% dimethyl sulphoxide (DMSO) solution in physiologic saline.

Thirty-five 8-week-old pregnant mice were injected with 4 mg/kg of VP-16 intraperitonially (i.p.) on GD 12, and each group including five dams were sacrificed by exsanguinations under ether anesthesia at 1, 2, 4, 8, 12, 24, and 48 hours after treatment (HAT), respectively. Twenty-one age-matched pregnant mice were injected i.p. with 1% DMSO solution on GD 12, and three dams were sacrificed in the same way at 1, 2, 4, 8, 12, 24, and 48 HAT, respectively. Fetuses were collected by Caesarian section from dams.

The protocol of the present study was approved by

the Animal Use and Care Committee of the Graduated School of Agricultural and Life Sciences, the University of Tokyo.

Histopathology

The fetuses obtained from the dams as scheduled were fixed in 10% neutral-buffered formalin and embedded in paraffin. Four-μm paraffin sections were then stained with hematoxylin and eosin (HE) for histopathological examination.

Immunohistochemistry

Immunohistochemical staining was carried out by LSAB method. Anti-cleaved caspase-3 antibody was obtained from Cell Signaling Technology., USA, and anti-proliferating cell nuclear antigen (PCNA) antibody was purchased from Novacostra Laboratories, UK. Paraffin sections were deparaffinized and immersed in 10mM citrate buffer, pH 6.0, and autoclaved for 10 min at 121°C. After washing in Tris-buffered saline (TBS), the sections were placed in 0.3% H_2O_2-containing methanol for 30 min to inactivate endogenous peroxidase. After incubation in skimmed milk at 37°C for 40 min to reduce non-specific staining, the sections were reacted with primary antibodies at 4°C overnight, with secondary antibody at room temperature for 40 min, and then with peroxidase-labeled streptoavidine (Dako, CA) at room temperature for 40 min, respectively. The sections were visualized by peroxidase-diaminobenzidine (DAB) reaction and then counterstained with methyl green.

In situ detection of fragmented DNA (apoptosis)

DNA fragmentation was examined on the paraffin sections by a modified TUNEL (Terminal deoxynucleotidyl Transferase Biotin-dUTP Nick End Labeling) method, which was first proposed by Gavrieli et al. (1992) and has been widely used for the detection of apoptotic cells. A commercial apoptosis detection kit (ApopTag® Peroxidase *In situ* Apoptosis Detection Kit; Chemicon, CA) was used in the present study. In brief, multiple fragmented DNA 3'-OH ends on a deparaffinized section were labeled with digoxigenin-dUTP in the presence of terminal deoxynucleotidyl transferase (TdT). Peroxidase-conjugated anti-digoxigenin antibody was then reacted with the section. Apoptotic nuclei were visualized by diaminobenzidine (DAB) reaction. The sections were then counterstained with methyl green.

Electron microscopy

Some fetal brain tissues were subjected to electron microscopic examination. Small pieces of the tissues were fixed in 2% glutaraldehyde in 0.1M phosphate buffer (pH 7.4), postfixed in 1% osmium tetroxide in the same buffer, and embedded in an epoxy resin (Oken, Shoji Co., Tokyo). Semithin sections were stained with toluidine blue for light microscopic survey. Ultrathin sections of selected areas were then double-stained with uranyl acetate and lead citrate, and observed using a JOEL 1200 EX electron microscope (Nippon Denshi Co., Ltd., Tokyo).

Cell counting

The number of mitotic cells in the ventricular zone (VZ) of telencephalon, was counted on one HE-stained section each for randomly chosen two fetuses per dam. TUNEL-positive and cleaved caspase-3-positive neuroepithelial cells in the telencephalon were counted on one immunostained section each for six fetuses per dam. One thousand cells were counted on each section under a light microscope (X400). Values were expressed as mean ± standard deviation (SD) at each point of examination, and statistical analysis was done by Student's t-test.

Results

There were no significant differences in body weight changes of fetuses between the VP-treated and control groups.

VP-16 administration induced histopathological changes in the fetal brain. Mitotic-index of neuroepithelial cells of the telencephalon began to decrease significantly at 2 and 4 HAT, and then recovered to the control level at 8 HAT (Fig. 1). At 4 HAT, there were only few mitotic neuroepithelial cells in the VZ of telencephalon.

Pyknotic cells in the telencephalon of VP-16 treated mice began to increase at 4 HAT, peaked at 12 HAT, gradually decreased at 24 HAT, and then returned to the control level at 48 HAT (Fig. 2). Pyknotic cells in the

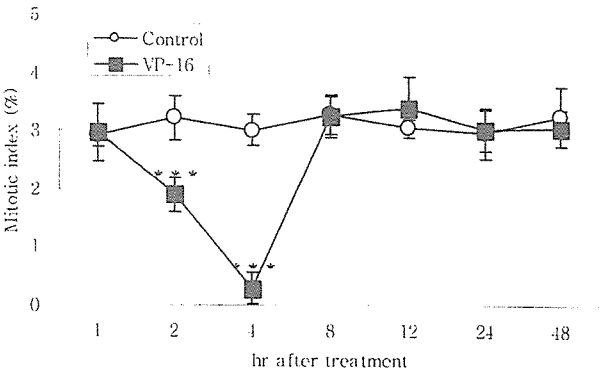

Fig. 1. Changes in the mitotic index (%) in the telencephalic wall of the fetal brain. Each value represents the mean ± SD of 2 fetuses obtained from each dam. ***p<0.001: Significantly different from control.

telencephalon were observed mainly in the ventral layer at 4 HAT and mainly in the middle and dorsal layers of the VZ at 8, 12, and 24 HAT, respectively (Fig. 2). Futhermore, in some fetuses, neuroepithelial cell arrangement was affected by the loss of pyknotic cells. These cells fell into the ventricular apace at 12 and 24 HAT.

Almost all of the pyknotic cells in the VP-16 treated fetal tissues were positive for TUNEL and cleaved caspase-3 (Figs. 3, 5). The time course of the number of TUNEL-positive cells in the telencephalic wall corresponded well to that of pyknotic cells. The number of TUNEL-positive cells increased significantly from 8 HAT, reached the peak at 12 HAT, decreased at 24 HAT, and then returned to the control level at 48 HAT (Fig. 4). Only a few TUNEL-positive cells were observed in controls. Cleaved caspase-3-positive cells in the VZ increased moderately at 4 HAT, peaked at 8 and 12 HAT, and decreased at 24 HAT (Fig. 6). On the other hand, PCNA-positive cells in the VZ slightly decreased only at 12 HAT compared to controls.

Electron-microscopically, the pyknotic cells were characterized by shrinkage of the cell body, condensation of nuclear chromatin and margination of condensed chromatin along the nuclear membrane (Fig 7a). Some apoptotic cells were fragmented into small pieces, which were frequently ingested by adjacent cells and macrophages (Fig 7b).

A similar but less prominent pyknotic changes were also observed in the diencephalon, mesencephalon, metencepahlon, spinal cord (only near the spinal canal area), and mesenchyme of limbs in VP-16-treated fetuses. Almost of these cells were also positive for TUNEL and cleaved caspase-3.

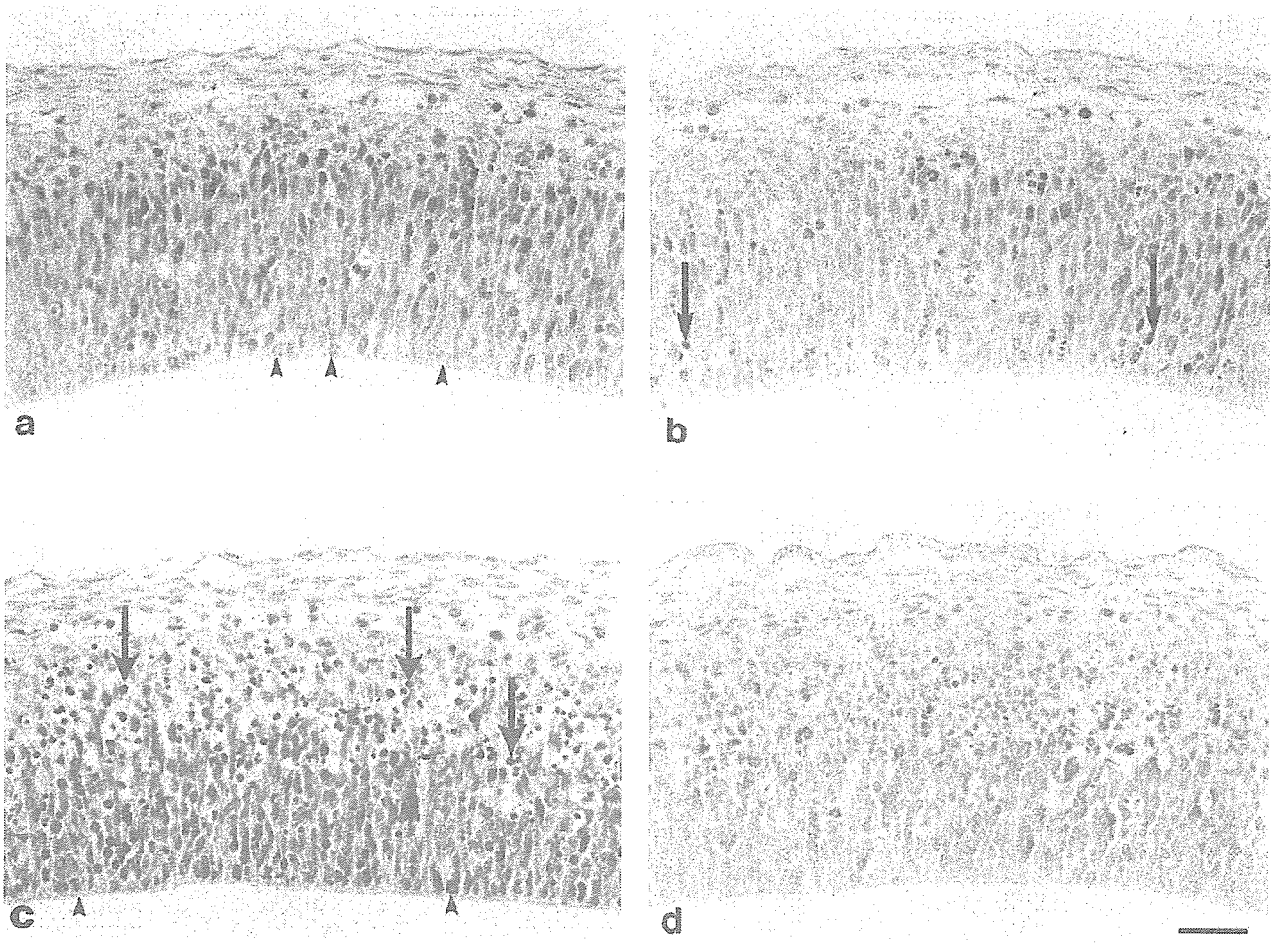

Fig. 2. Histological appearances of the telencephalic wall of a control fetus (a) and those of VP-16-treated fetuses at 4 HAT (b), 12 HAT (c), and 24 HAT (d). HE stain, bar: 31 μm. Pyknotic cells were observed from 4 HAT. The number of pyknotic cells peaked at 12 HAT, and then gradually decreased at 24 HAT. Arrowheads: mitotic cell; Arrows: pyknotic cell. x 400

Discussion

Etoposide (VP-16), a topoisomerase II inhibitor, has been widely used as an antitumor drug since 1970. VP-16 is also known as a genotoxic and teratogenic chemical. This study was focused on morphological characteristics of the fetal mouse brain lesions treated with VP-16 on GD 12.

Almost all of the nuclei of VP-16-induced pyknotic cells were positive for TUNEL stain and cleaved caspase-3. Activation of caspase-3 is an essential event for apoptosis, and it is either partially or totally responsible for the proteolytic cleavage of many key proteins during the apoptotic cascade such as the nuclear enzyme poly (ADP-ribose) polymerase (PARP) (Fernandes-Alnemri et al., 1994). Moreover, electron microscopic features of these cells accorded well with the ultrastructural characteristics of apoptotic cells (Ihara et al., 1998). TUNEL method, which can detect fragmented DNA *in situ*, is widely used for the evaluation of apoptotic cells. Even though some researchers have recently demonstrated that TUNEL technique may not be specific for apoptotic cells, and it also detects a small population of necrotic cells (de Torres et al., 1997; Levin et al., 1999), the detection of cleaved caspase-3 and ultrastructural morphology in the VP-16-treated fetal mouse brain in this study verified apoptotic changes. Therefore, it is reasonable to consider that the pyknotic cells observed in the fetal brain of the VP-16-treated fetuses are apoptotic ones.

Following VP-16 treatment to pregnant mice on GD 12, a marked decrease of mitosis of neuroepithial cells was observed in the VZ from 2 HAT to 4 HAT. The cleaved caspase-3-positive cells began to increase at 4 HAT, peaked at 8 and 12 HAT, and then decreased weakly at 24 HAT. This indicates that VP-16-induced apoptotic changes of neuroepithelial cells began to occur at 4 HAT. Decreased mitotic index before apoptotic

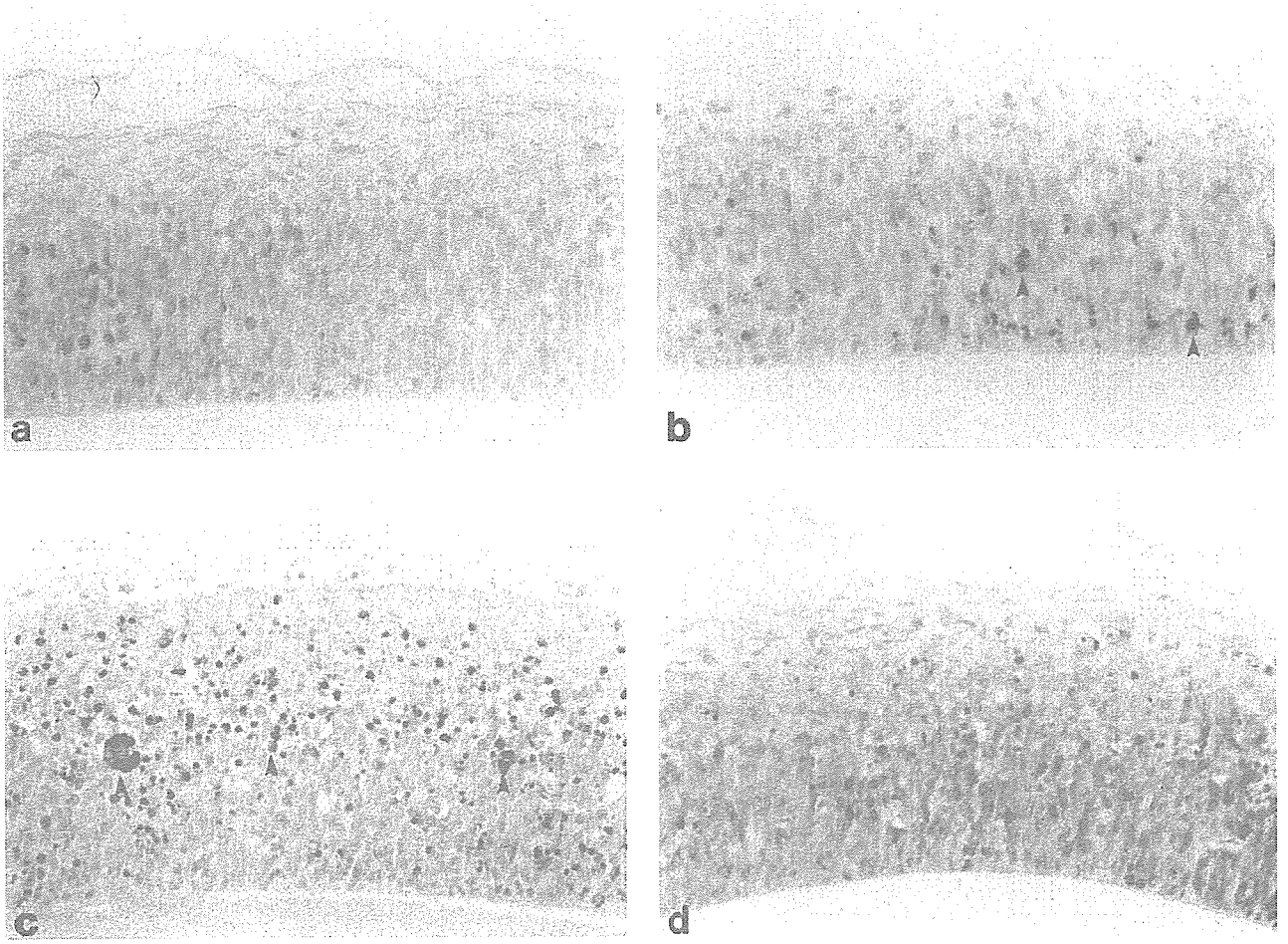

Fig. 3. TUNEL-positive cells in the telencephalic wall of the fetal brain of a control (**a**) and those of VP-16-treated fetuses at 4 HAT (**b**), 12 HAT (**c**), and 24 HAT (**d**). The number of TUNEL-positive cells began to increase from 4 HAT, peaked at 12 HAT, and decreased at 24 HAT. Arrowheads: TUNEL-positive cells. x 400

changes demonstrated in the present study suggested that the initiation of neuroepithelial damage might occur in the pre-mitotic phase of the cell cycle. Apoptotic neuroepithelial cells were mainly observed in the middle and dorsal layers of the VZ at 8, 12, and 24 HAT. It is reported that the neuroepithelial cells in the dorsal layer actively synthesize DNA (S-phase), and those of the middle layer are in the G1 or G2 phase of the cell cycle (Langman et al., 1966). VP-16 has also been reported to induce apoptosis throughout late G1/S or G1 arrest in mouse embryo fibroblasts (Attardi et al., 2004).

Apoptotic changes in neuroepithelial cells of the fetal brain were reported in rats and mice following prenatal treatment with other teratogenic drugs such as 5-azacytidine (Lu et al., 1998), ethylnitrosourea (Katayama et al., 2000), hydroxyurea (Woo et al., 2003), and 1-ß-arabinofuranosylcytosine (Yamauchi et al, 2003). The present study showed that VP-16 can also

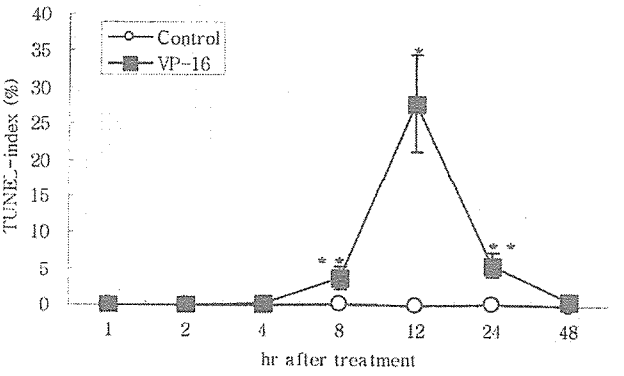

Fig. 4. Changes in the TUNEL-index (%) in the telencephalic wall of the fetal brain. Each value represents the mean ± SD of 6 fetuses obtained from each dam. *p<0.05: Significantly different from controls, **p<0.01: significantly different from controls.

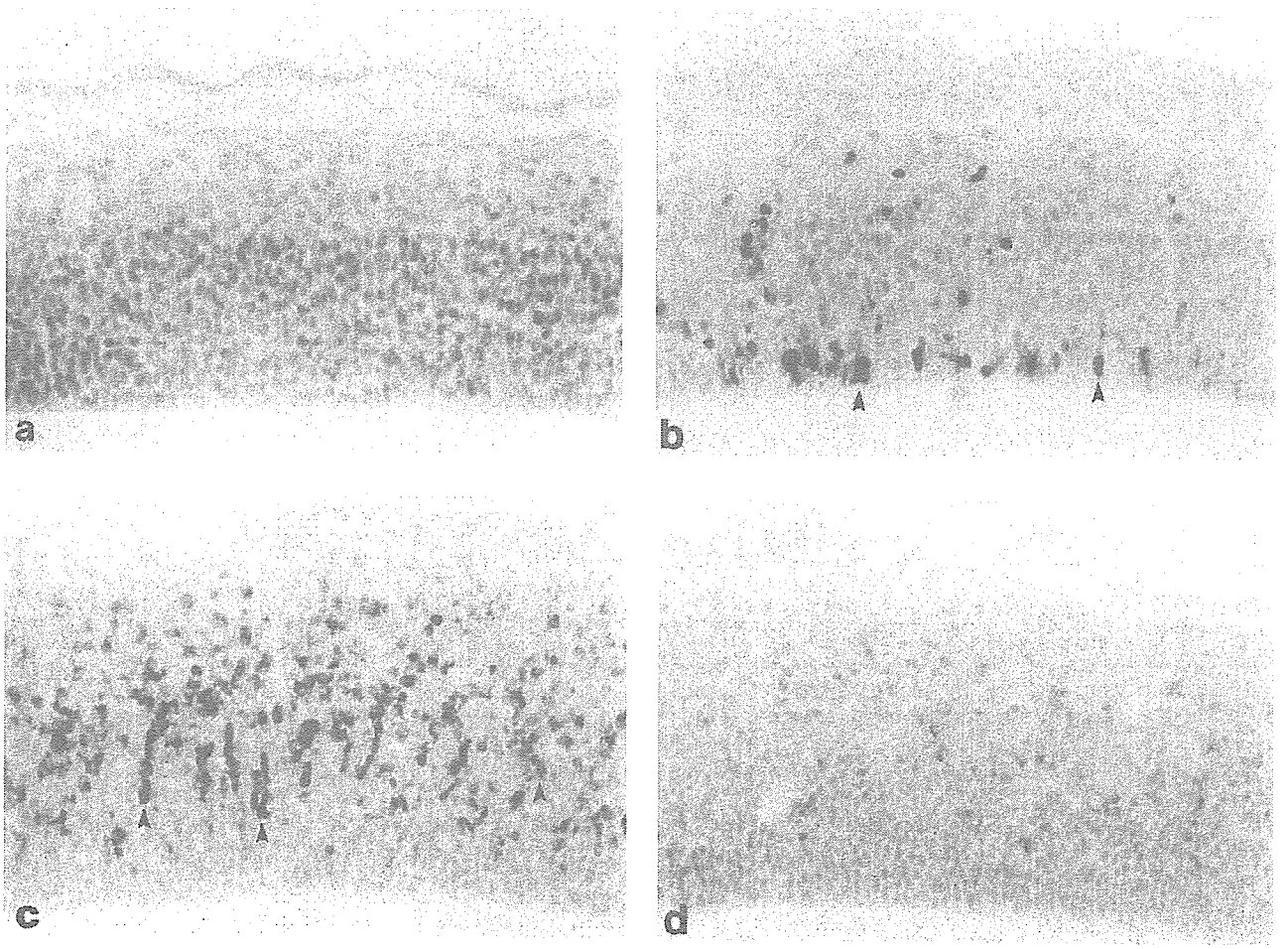

Fig. 5. Immunostaining for cleaved caspase-3 in the telencephalic wall of a control fetus **(a)** and of VP-16-treated fetuses at 4 HAT **(b)**, 12 HAT **(c)**, and 24 HAT **(d)**. The cleaved caspase-3 positive cells began to increase at 4 HAT, peaked at 8 and 12 HAT, and decreased at 24 HAT. Arrowheads: cleaved caspase-3-positive cell. x 400

induce similar morphological changes in the fetal brain. These findings suggest that the fetal brain in the organogensis phase might be very sensitive to such teratogenic chemical exposures.

VP-16 alters microtubule assembly, and mainly poisons topoisomerase II by increasing the steady-state concentrate of their covalent DNA cleavage complexes. Therefore this action converts topoisomerases into physiological toxins that cause high levels of transcript of transient-associated DNA breaks in the genome (Chen and Liu, 1994; Jesen and Sehested, 1997; Hande, 1998). When VP-16 was removed, DNA breakage was quickly repaired (Wozniak and Ross, 1983; Hande, 1998). Plasma half –life of VP-16 is less than 2 hr in mice when injected i.p. and 6.4 hr in human via intravenous route (Dorr et al., 1989; Hande, 1998). According to our present results, rapid recovery from VP-16-induced cellular damage caused by VP-16 corresponded well to the pharmacokinetics of VP-16.

Single injection of VP-16 (1.5, 2, and 3 mg/kg) at the early gestation period caused embryocidal or more severe teratogenic effects such as major skeletal malformation and/or various cranial abnormalities (Sieber et al., 1978). In the present study, administration of VP-16 of 4 mg/kg to pregnant mice on GD 12 (fetal organogenesis phase) induced apoptotic cell death only in the fetal CNS and mesenchyme of limbs. Accordingly, VP-16 administration into dams might induce various embryotoxic and teratotoxic effects, depending on the

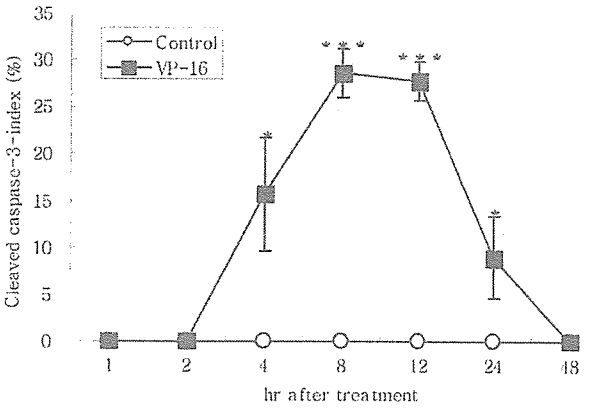

Fig. 6. Changes in the cleaved caspase-3-index (%) in the telencephalic wall of the fetal brain. Each value represents the mean ± SD of 6 fetuses obtained from each dam. *p<0.05: significantly different from control, ***p<0.001: significantly different from control.

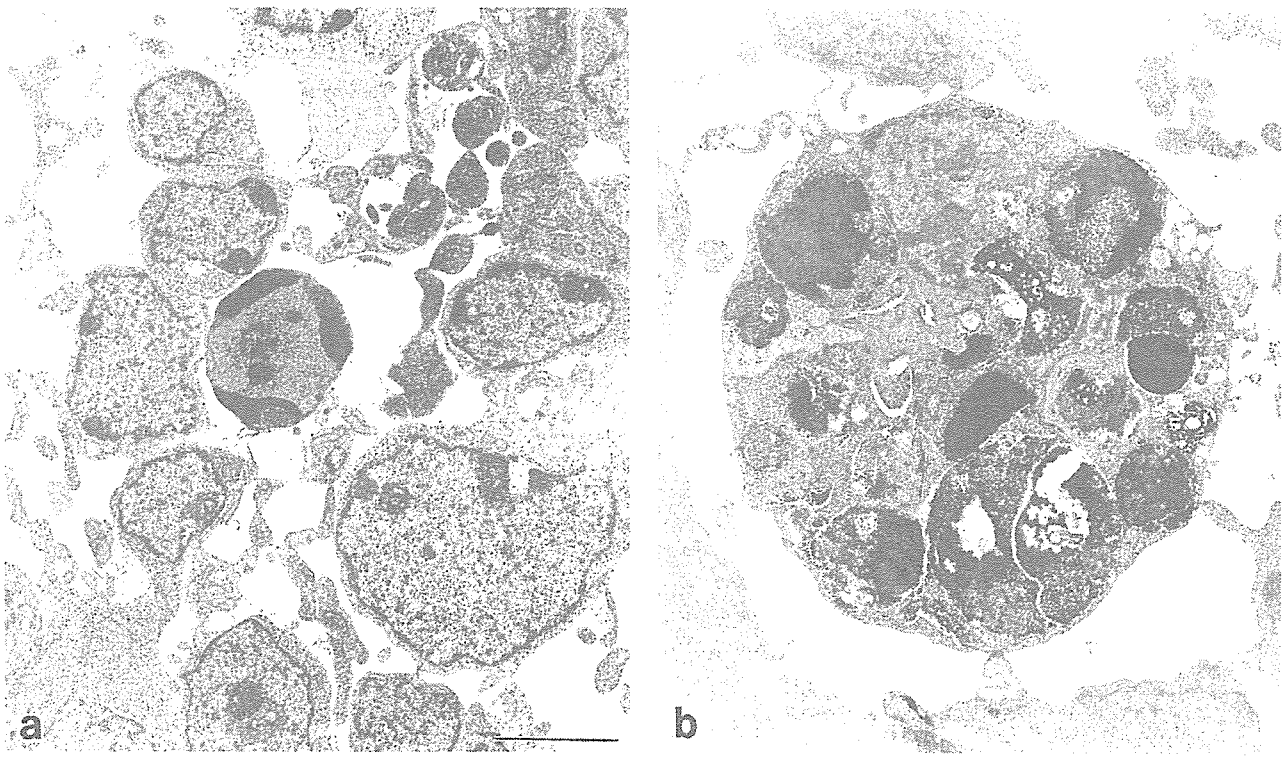

Fig 7. Electron microscopy of the telencenphalic wall of the VP-16-treated mouse fetal brain. **a.** An apoptotic cell at the center shows margination of condensed nuclear chromatin along the nuclear membrane. **b.** Apoptotic bodies are ingested by a macrophage. Bar: 2.0 μm.

gestational day of VP-16 injection.

In conclusion, cellular damage in the fetal brain obtained from pregnant mice treated with VP-16 on GD 12 was apoptotic cell death. The present results offer a clue for studies on the mechanisms of fetotoxicity and teratogenicity induced by VP-16. Further studies on gene expression profiles are now in progress in the fetal brain after VP-16 administration to dams.

Aknowledgements. The authors appreciate Akira Yososhima, Department of Veterinay Pathology, the University of Tokyo, for his excellent technical assistant for electronmicroscopy.

References

Attardi L.D., Vries A. and Jacks T. (2004). Activation of the p53-dependent G1 checkpoint response in mouse embryo fibroblasts depends on the specific DNA damage inducer. Oncogene 23, 973-980.

Chen A.Y. and Liu L.F. (1994). DNA topoisomerases: essential enzymes and lethal targets. Annu. Rev. Pharmacol. Toxicol. 34, 191-218.

de Torres C., Munell F., Ferrer I., Reventos J. and Macaya A. (1997). Identification of necrotic cell death by the TUNEL assay in the hypoxic-ischemic neonatal brain. Neurosci. Lett. 230, 1-4.

Dorr R.T., Liddil J.D., von Hoff D.D., Sobe M. and Osborne C.K. (1989). Antitumor activity and murine pharmacokinetics of paraental acronycine. Cancer Res. 49, 340-344.

Fernandes-Alnemri T., Litwack G.. and Alnemri G.S. (1994). CPP32, a novel human apoptotic protein with homology to Caenorhabditis elegans cell death protein Ced-3 and mammalian interleukin-1 beta-converting enzyme, J. Biol. Chem. 269, 30761-30764.

Gavrieli Y., Sherman Y. and Ben-Sasson S.A. (1992). Identification of programmed cell death in situ via specific labeling of nuclear DNA fragment. J. Cell Biol. 119, 493-501.

Hande K.R. (1998). Etoposide: four decades of development of topoisomerase inhibitor. Eur. J. Cancer 34, 1514-1521.

Ihara T., Yamamoto T., Sugamata M., Okumura H. and Ueno Y. (1998). The progress of ultrastuctural changes from nuclei to apoptotic body. Virchows Arch. 433, 443-447.

Jensen P.B. and Sehested M. (1997). DNA topoisomerase II rescued by catalytic inhibitors: a new strategy to improve the antitumor selectivity of etoposide. Biochem. Pharmacol. 54, 755-759.

Katayama K., Ishigami N., Uetsuka K., Nakayama H. and Doi K. (2000). Ethylnitrourea (ENU)-induced apoptosis in the fetal tissues. Histol. Histopathol. 15, 707-711.

Langman J., Guerrant R.L. and Freeban B.G. (1966). Behavior of neuroepithelial cells during closure of the neural tube. J. Comp. Neurol. 132, 355-374.

Levin S., Bucci T.J., Cohen S.M., Fix A.S., Hardisty J.F., LeGrand E.K., Maronpot P.R. and Trump B.F. (1999). The nomenclature of cell death: Recommendation of an ad hoc committee of the society of toxicological pathologists. Toxicol. Pathol. 27, 484-490.

Lu D.P., Nakayama H., Sinozuka J., Uetsuka K., Taki R. and Doi K. (1998). 5-Azacytidine-induced apoptosis in the central nervous system of developing rat fetuses. J. Toxicol. Pathol. 11, 133-136.

Sieber S.M., Whang-Peng J., Botkin C. and Knutsen T. (1978). Teratogenic and cytogenetic effects of some plant-derived antitumor agents (vincristine, colochicine, maytasine, VP-16-213 and VM-216) in mic. Teratology 18, 31-48.

Woo G.H., Katayama K., Jung J.Y., Uetsuka K., Bak E.J., Nakayama H. and Doi K. (2003). Hydroxyurea (HU)-induced apoptosis in the mouse fetal tissues. Histol. Histopathol. 15, 387-392.

Wozniak A.J. and Ross W.E. (1983). DNA damages a basis for 4-demethyl-epipodophyllotoxicity. Cancer Res. 43, 120-124

Yamauchi H., Katayama K., Yososhima A., Uetsuka K., Nakayama H. and Doi K. (2003). 1-ß-Arabinofuranosylcytosine(Ara-C)-induced apoptosis in the rat fetal tissues and placenta. J. Toxicol. Pathol. 16, 223-229.

Accepted November 2, 2005

Available online at www.sciencedirect.com
SCIENCE DIRECT
Experimental Neurology 198 (2006) 154–166
Experimental Neurology
www.elsevier.com/locate/yexnr

Cell cycle and cell death regulation of neural progenitor cells in the 5-azacytidine (5AzC)-treated developing fetal brain

Masaki Ueno*, Kei-ichi Katayama, Hirofumi Yamauchi, Hiroyuki Nakayama, Kunio Doi

Department of Veterinary Pathology, Graduate School of Agricultural and Life Sciences, The University of Tokyo, 1-1-1 Yayoi, Bunkyo-ku, Tokyo 113-8657, Japan

Received 28 April 2005; revised 22 November 2005; accepted 22 November 2005
Available online 19 January 2006

Abstract

In the developing brain, neural progenitor cells are susceptible to many extrinsic stresses, including DNA damage. We treated pregnant rats with 5-azacytidine (5AzC), a DNA demethylating and damaging agent, to investigate the cellular responses of the fetal brain, focusing on the regulation of proliferation and cell death. 5AzC first induced the accumulation of cells in abnormal mitosis, G2-phase accumulation, and then apoptosis of the neural progenitor cells. Most of the apoptotic cells were in G1 phase. Cell cycle transition studies suggested that G2/M progression was blocked, after which the cells moved to G1 phase or underwent apoptosis. p53, a key factor for response to DNA damage, and some of its target genes showed increased expression in Western blot and DNA microarray analyses. In 5AzC-treated fetal brains of p53-deficient mice, apoptosis did not occur, although G2/M accumulation was induced. These results suggest that, in the developing brain, apoptosis is p53-dependent but that another mechanism governs the G2/M checkpoint. The G2/M regulator, Cdc2, was activated by dephosphorylation through G2/M accumulation, suggesting accelerated entry into mitosis leading to accumulation of cells showing abnormal mitosis. Furthermore, some cells may have died due to mitotic catastrophe. Throughout brain development, various cell cycle and cell death regulation mechanisms provide neural progenitor cells with options for defense from DNA damage.

Keywords: Apoptosis; 5-azacytidine; Cell cycle arrest; DNA damage; Interkinetic nuclear migration; Mitotic catastrophe; Neural progenitor cell; p53; Ventricular zone

Introduction

Environmental stresses and stimuli can induce deleterious effects on brain development. The fetal central nervous system (CNS) is sensitive to diverse environmental factors because a large number of processes occur during an extended period of development, and fetal neural damage is an important issue affecting the completion of normal CNS development (Rodier, 1995; Mendola et al., 2002; Costa et al., 2004).

In the developing brain, multipotent neural progenitor cells proliferate in the ventricular zone (VZ), after which they differentiate into neural cells, i.e., neurons, astrocytes, and oligodendrocytes (Rao, 1999; Qian et al., 2000; Temple, 2001). In the early developmental stage, they form a pseudostratified epithelium in the VZ, so they also are called neuroepithelial cells. The nuclei of proliferating neural progenitor cells undergo a characteristic migration–interkinetic nuclear migration (or "elevator movement")–in the VZ, in which the positions of nuclei are correlated with their cell cycle phase (Takahashi et al., 1995; Fujita, 2003). In brief, the S phase nuclei located in the outer area of the VZ translocate inward during G2 phase, and mitosis occurs at the ventricular surface. Then, the nuclei migrate outward during G1 and enter S phase again (Fig. 7A). In this way, neural progenitor cells proliferate.

The balance between proliferation and cell death (apoptosis) is important for correct development of the brain (Oppenheim, 1991; Blaschke et al., 1996; Thomaidou et al., 1997). Moreover, the regulation of this balance also seems to be important during damage due to extrinsic stresses, particularly that from anti-proliferative stimuli. However, it remains unclear how neural progenitor cells in the fetal brain react toward extrinsic stresses, especially regarding the regulation of proliferation and cell death, while the organ is still developing.

5-Azacytidine (5AzC) is an agent that has two characteristic effects that interfere with the brain development, i.e. disturbance

* Corresponding author. Fax: +81 3 5841 8185.
E-mail address: ms-ueno@umin.ac.jp (M. Ueno).

0014-4886/$ – see front matter © 2005 Elsevier Inc. All rights reserved.
doi:10.1016/j.expneurol.2005.11.024

of DNA methylation and DNA damage. During the development of the CNS as well as other organ systems, DNA methylation is a key step for regulating gene expression (Sun et al., 2003), and agents such as 5AzC may disturb gene expression, and subsequently organogenesis, through their DNA demethylating effects. 5AzC also is thought to act as a DNA damaging agent (Juttermann et al., 1994: Karpf et al., 2001), and DNA damage causes serious abnormalities in the developing brain (Gao et al., 1998; Vinson and Hales, 2002: D'Sa et al., 2003). In our previous study, we demonstrated that 5AzC treatment of the pregnant rats prompted neural progenitor cells in the fetal brain to undergo apoptotic cell death; the treatment also led to delayed migration of nuclei, suggesting that cell cycle arrest might occur (Ueno et al., 2002a,b). In addition, our data indicated that these events might be dependent on p53, a tumor suppressor protein, and its transcriptional target genes such as $p21^{waf1/cip1}$. p53 is known to play a key role in the induction of cell growth arrest and apoptosis in response to DNA damage (May and May, 1999; Lakin and Jackson, 1999). However, despite these observations, it was unclear at which cell cycle phase the neural progenitor cells arrested and underwent apoptosis due to 5AzC treatment.

In the present study, we exposed fetal rat brains to 5AzC to examine how the neural progenitor cells response to extrinsic stresses, focusing on the regulation of apoptosis and cell cycle kinetics. We used flow cytometric methods for investigating alterations in cell cycle distribution and assessing the cell cycle position of apoptotic cells. Furthermore, we evaluated alteration of gene expression by using DNA microarray technology to reveal various mechanisms underlying cellular responses to 5AzC. In our examination, we focused on the role of p53 in the regulation of apoptosis and the cell cycle, and we used p53-knockout mice to confirm these points. We found that both p53-dependent and -independent mechanisms were involved in the regulation of apoptosis and the cell cycle of 5AzC-treated neural progenitor cells.

Materials and methods

All procedures were approved by the Animal Care and Use Committee of the Graduate School of Agricultural and Life Sciences, The University of Tokyo.

Animals

Pregnant Jcl:Wistar rats were obtained from Japan CLEA (Tokyo, Japan). $p53^{+/-}$ mice (C57BL/6 TSG-p53 N5 Targeted Mutation) were purchased from Taconic (Germantown, NY). Heterozygous mice were crossed to generate wild-type, heterozygous, and homozygous gene-disrupted mice. Endogenous and disrupted genes were detected by polymerase chain reaction analysis of tail DNA extracts, as described by Timme and Thompson (1994).

Chemicals

5AzC and 5-bromo-2′-deoxyuridine (BrdU) were obtained from Sigma (St. Louis, MO).

Treatments for Wistar rats

On day 13 of gestation pregnant, rats were injected intraperitoneally (i.p.) with 10 mg/kg of 5AzC and then euthanized at 1, 3, 6, 9, and 12 h after treatment. The dose was selected according to that of a previous study, in which 10 mg/kg of 5AzC caused high induction of neural cell apoptosis and low fetal mortality (Lu et al., 1998). As controls, pregnant rats were injected with an equivalent volume of saline and euthanized at 1, 3, 6, 9, and 12 h after treatment. Collected fetuses underwent histopathological examination, and cell cycle, DNA microarray, and Western blot analyses.

Treatments for p53-knockout mice

Pregnant mice were injected i.p. with 10 mg/kg of 5AzC on day 12 of gestation and euthanized at 6 and 12 h after treatment. As controls, dams were injected i.p. with an equivalent volume of saline on day 12 of gestation and were euthanized at 6 h after treatment. Collected fetuses were subjected to histopathological examination and cell cycle analysis.

Histopathological examination and immunohistochemistry

Collected fetuses were fixed in 10% neutral-buffered formalin and embedded in paraffin. Paraffin sections (thickness, 4 μm) were stained with hematoxylin and eosin for histopathological examination. The dorsal telencephalic wall was mainly examined.

Some of the sections underwent immunohistochemical staining for cleaved caspase-3 and phospho-histone H3 by the LSAB method with streptavidin (Dako, Carpinteria, CA). Rabbit anti-cleaved caspase-3 polyclonal antibody (Cell Signaling Technology, Beverly, MA) and rabbit anti-phospho-histone H3 polyclonal antibody (Cell Signaling Technology) were used as the primary antibodies and biotin-labeled goat anti-rabbit IgG (Kirkegaard and Perry, Gaitherburg, MD) as the secondary antibody.

Staining for p53 and $p21^{waf1/cip1}$ was performed with an Envision+ Kit (Dako), as previously reported (Ueno et al., 2002a). Rabbit anti-p53 polyclonal antibody (Santa Cruz Biotechnology, Santa Cruz, CA) and mouse anti-p21 monoclonal antibody (Pharmingen, San Diego, CA) were used as the primary antibodies. The positive signals were visualized using a peroxidase-diaminobenzidine reaction, and then the sections were counterstained with methyl green.

Cell cycle analysis

Telencephalons of two or three fetuses from each dam (1 to 12 h after treatment, and controls) were obtained carefully under stereoscopic microscopy and then prepared for flow cytometric analysis. The cells isolated from the telencephalons from each dam were resuspended in HBSS. The concentration of the resuspended cells was adjusted to $1–2 \times 10^6$. They were centrifuged for 5 min at $1500 \times g$ at 4°C, and the supernatant was discarded. After being washed in Dulbecco's PBS (dPBS), the cells were fixed in 70% ethanol at 4°C overnight. Cells then

were washed in dPBS and incubated with ribonuclease A (RNase A; 250 μg/ml, Sigma) for 40 min at 37°C. Cells were stained with propidium iodide (PI; 50 μg/ml, Sigma) for 30 min on ice. Cell cycle analysis was performed using the FACS Callibur system (Becton Dickinson, Mountain View, CA), and cell cycle distribution was analyzed using the Cell Quest program (Becton Dickinson).

Detection of BrdU-positive cells in the cell cycle

Pregnant rats on day 13 of gestation were injected i.p. with 10 mg/kg of 5AzC and 20 mg/kg of BrdU concurrently and then euthanized at 1, 3, 6, 9, and 12 h after treatment. As controls, pregnant rats were injected only with BrdU and euthanized at 1, 3, 6, 9, and 12 h after treatment. Collected fetuses underwent flow cytometric analysis to investigate the transition of BrdU-incorporated cells in the cell cycle. Cells isolated from two or three fetal telencephalons were resuspended and then washed and fixed using the same method described for cell cycle analysis. After being fixed in 70% ethanol, the cells were washed with dPBS and then resuspended for 30 min at room temperature (RT) in 2 M HCl containing 0.5% Triton X-100. After being neutralized in 0.1 M $Na_2B_4O_7$, the cells were incubated with FITC-labeled anti-BrdU monoclonal antibody (Pharmingen, San Diego, CA) for 30 min at RT. They then were resuspended in dPBS containing PI (10 μg/ml) for 30 min on ice and analyzed using the FACS Callibur system and Cell Quest program (Becton Dickinson).

Detection of fragmented DNA

Fragmented DNA was detected with an APO-BrdU Kit (Pharmingen). The manufacturer's protocol was followed with minor modifications. Cells were isolated from three rat fetal telencephalons from each dam (9 and 12 h after treatment, and controls) as for cell cycle analysis and first fixed in 1% paraformaldehyde in dPBS for 15 min on ice. After being washed with dPBS, they were fixed in 70% ethanol at 4°C for one or two overnights. Cells then were washed in the Wash Buffer from the kit and incubated in the DNA Labeling Solution for 60 min at 37°C. In this solution, the multiple fragmented DNA 3′-OH ends in the nuclei were labeled with Br-dUTP in the presence of terminal deoxynucleotidyl transferase (TdT). After being washed in Rinse Buffer, cells were incubated for 30 min at RT in Antibody Staining Solution containing FITC-labeled anti-BrdU antibody and then stained with PI/RNase A solution for 30 min at RT. FITC-positive apoptotic cells were detected and analyzed using the FACS Callibur system (Becton Dickinson) and Cell Quest program (Becton Dickinson).

RNA extraction and microarray analysis

Microarray expression analysis was performed using the Affymetrix GeneChip system (Santa Clara, CA) according to the manufacturer's instructions. Six to eight rat fetal telencephalons were acquired from each dam (6, 9, or 12 h after treatment, and controls, $n = 2$ dams per time point), and total RNA was extracted with the RNeasy Mini Kit (Qiagen, Germantown, MD). The quality and quantity of the extracted RNA samples were examined by agarose gel electrophoresis. Then, double-stranded cDNA was synthesized from total RNA. The first cDNA strand was prepared from 10 μg of total RNA by using SuperScript II RNase H^- Reverse Transcriptase (Invitrogen) and the T7-$(dT)_{24}$ primer (primer sequence, 5′-GGCCAGTGAATTGTAATACGACTCACTATAGG-GAGGCGG-$[dT]_{24}$-3′, Amersham Bioscience, Tokyo, Japan). The second strand was synthesized using the SuperScript Double-stranded cDNA Synthesis Kit (Invitrogen). Then, biotin-labeled cRNA was synthesized from the double-stranded cDNA by using the Enzo High-yield RNA Transcription Labeling Kit (Enzo Diagnostics, NY) and purified with the RNeasy Mini Kit (Qiagen). Twenty micrograms of biotin-labeled cRNA was then fragmented in a fragmentation buffer. Fragmented cRNA was mixed in a hybridization solution prepared with a GeneChip Eukaryotic Hybridization Control Kit (Affymetrix) and hybridized to the Affymetrix Rat Expression Array 230A for 16 h at 45°C while being rotated at 60 rpm in a GeneChip Hybridization Oven 640 (Affymetrix). The chips were then washed and stained automatically with a Fluidics Station (Affymetrix) and scanned with the GeneArray Scanner (Hewlett Packard, Palo Alto, CA).

Microarray data analysis

The microarray imaging data were analyzed using MicroarraySuite ver. 5.0 (Affymetrix). After hybridization intensity data were captured, the intensity values of each probe were calculated automatically. Data were compared between the treated and control groups. Prior to comparing any two measurements, scaling and normalizing procedures were performed. In the case of a pairwise comparison of two array results, the patterns of change of the whole probe set were used to make a qualitative call (called difference call) of "Increase (I)", "Decrease (D)", "Marginal increase (MI)", "Marginal decrease (MD)", or "No change (NC)", in which statistical analysis was done following the manufacturer's guide (MicroarraySuite ver 5.0 User's Guide). We then extracted the groups of genes corresponding to I, MI, D, or MD in both samples at each time point and performed pathway analyses as mentioned below. The fold change in gene expression was derived from the ratio of the average difference from one experimental array compared with a control array.

The extracted genes underwent signal pathway analysis with GenMAPP (http://www.GenMAPP.org). This analysis involves the uploading of gene expression data onto known biologic pathways and a list of genes that is categorized with gene functions. Data regarding each gene are easily visualized, including its change in expression and roles in various signal cascades.

Real-time PCR

Some of the total RNA extracted for microarray analysis was subjected to reverse transcription for the first-strand cDNA synthesis by using an oligo $(dT)_{12-18}$ primer and

SuperScript II RNase H⁻ Reverse Transcriptase (Invitrogen). Real-time PCR was performed using oligonucleotide primers sets corresponding to the cDNA sequences of *cyclin B1*, *Cdc20*, and *glyceraldehyde-3-phosphate dehydrogenase* (*GAPDH*). Sense and antisense primers were as follows: *cyclin B1*, sense 5′-CAGAGGTGGAACTGGATGAGC-3′ and antisense 5′-GGGCTTGGAGAGGGAGTATCA-3′; *Cdc20*, sense 5′-AGGAGGTACCAGTGACCGACA-3′ and antisense 5′-ACCAGAGGATGGAGCACACC-3′; and *GAPDH*, sense 5′-CCTGCACCACCAACTGCTTAG-3′ and antisense 5′-CATGGACTGTGGTCATGAGCC-3′. In brief, 25 μl of reaction mixture containing 12.5 μl SYBR Green Real-time PCR Master Mix (Toyobo, Osaka, Japan), 0.2 μM each of the sense and antisense primers, and 1 μl of the cDNA sample was preheated at 95°C for 3 min and then underwent 40 cycles of amplification (denaturation at 95°C for 15 s, annealing and extension at 60°C for 1 min) by using the ABI PRISM 7900 HT Sequence Detection System (Applied Biosystems, Foster City, CA). Relative intensity against *GAPDH* was calculated, and fold change relative to the control was represented as the mean ± standard deviation (SD) of 2 dams.

Western blotting

Four or five rat fetal telencephalons (3 to 12 h after treatment, and controls) were homogenized in a solution of 20 mM Tris–HCl (pH 7.4) containing 150 mM NaCl, 1 mM PMSF, 1% aprotinin, 2 mM EDTA, 2 mM Na_3VO_4, 1% NP-40, 0.1% SDS, and 1 mM DTT and centrifuged at 12,000 × *g* for 20 min at 4°C. Approximately 30 μg of extract was loaded per lane of a 10% SDS-PAGE gel, electrophoresed, and transferred to a PVDF membrane (Bio-Rad, Hercules, CA). Blots first were probed with antibodies to p53 (Santa Cruz), Chk2 (Santa Cruz), $p21^{waf1/cip1}$ (Pharmingen), cyclin B1 (NeoMarkers, Fremont, CA), Cdc2 (Cell Signaling Technology), phospho-Cdc2 (Tyr16) (Cell Signaling Technology), and β-actin (Sigma). After incubation with the appropriate secondary antibody conjugated to horseradish peroxidase (Amersham, Buckinghamshire, UK), detection was performed with the ECL Plus kit (Amersham).

Results

Histopathological changes

Histopathological changes induced by 5AzC-treatment were almost same in the VZ of all area of telencephalon, i.e. telencephalic wall and basal ganglia. In this study, therefore, we chose dorsal telencephalic wall to observe the changes.

We first counted mitotic cells with phospho-histone H3, a marker of mitosis. Although this antigen is also present in late G2 phase, we counted only the phospho-histone-H3-positive cells which have mitotic figures. At 6 h after 5AzC treatment, the number of mitotic cells positive for phospho-histone H3 was increased in the VZ along the ventricle (Figs. 1A and B). These

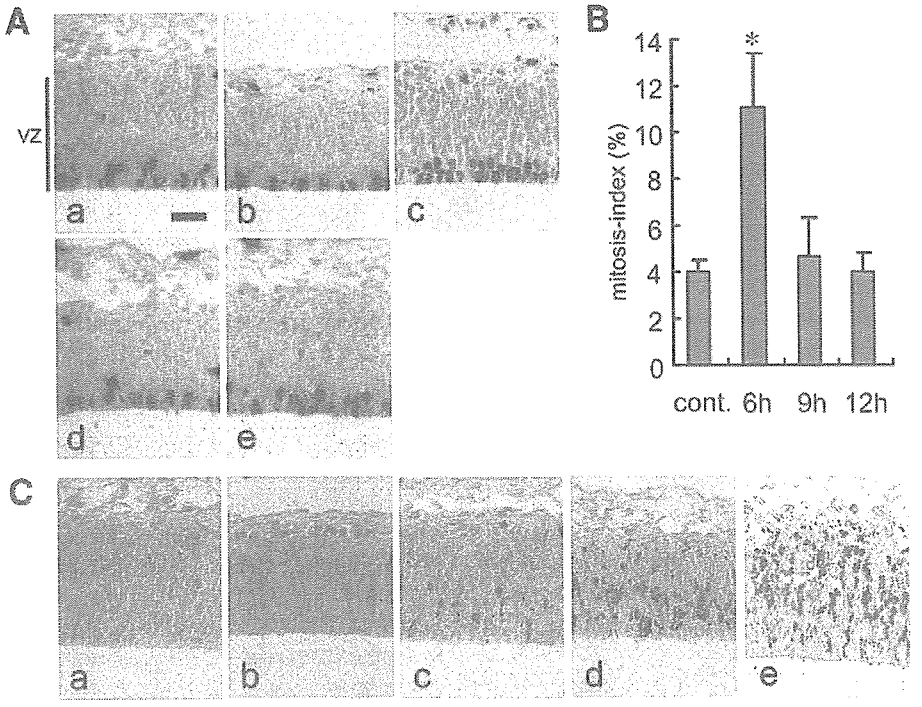

Fig. 1. Histopathological changes in the VZ of dorsal telencephalic wall of rat fetus. (A) Staining for phospho-histone H3, a mitotic marker (a: control (12 h), b: 3 h, c: 6 h, d: 9 h, and e: 12 h). Mitoses are observed mainly along the ventricular surface throughout the experimental period. Mitotic cells remarkably increased at 6 h (c). (B) The mitosis index (%) of neural progenitor cells at the ventricular surface. The indices (%; the number of phospho-histone-H3-positive cells with mitotic figures/500 cells in the VZ) are represented as the mean ± SD ($n = 3$). *$P < 0.05$; significantly different from the control (12 h) (Student's *t* test). Mitotic cells remarkably increased at 6 h and then decreased to the control level. (C) Staining for cleaved caspase-3, an apoptosis marker (a: control (12 h), b: 3 h, c: 6 h, d: 9 h, and e: 12 h). The number of cleaved caspase-3-positive cells appeared at 6 h and increased from 9 to 12 h. Scale bar: 50 μm.

results coincide with those of our previous study, in which we observed aberrant accumulation of mitotic cells with abnormal morphology along the ventricle (Ueno et al., 2002b). These cells gradually decreased in number after 6 h. From 6 to 12 h, the number of pyknotic cells, which had the morphological characteristics of apoptotic cells (Ueno et al., 2002b), increased among the neural progenitor cells in the VZ. Immunohistochemically, the pyknotic cells were stained positively for cleaved caspase-3 (Fig. 1C), which is known to be involved in neural cell apoptosis during development as well as in the apoptosis of neurons induced by DNA-damaging agents (Kuida et al., 1996; Keramaris et al., 2000).

Cell cycle analysis

In E12 to E13 mice, about 70% of cells in the fetal telencephalon are neural progenitor cells (D'Sa-Eipper and Roth, 2000), so we believe that the cells we analyzed reflected the cell cycle distribution of neural progenitor cells (Fig. 2). Furthermore, most of the neural progenitor cells that we analyzed were thought to localize in the VZ, rather than the subventricular zone (SVZ), the other area where neural progenitor cells proliferate, because the SVZ is not yet prominent in E13 rat (Fig. 1A).

The cell cycle distribution from 1 to 3 h after 5AzC treatment did not markedly differ from that of the control. At 6 h, the number of cells in G2/M phase increased (control, 8.8 ± 0.7%; 5AzC, 15.0 ± 0.9%) and that in G0/G1 decreased (control, 72.5 ± 1.4%; 5AzC, 61.6 ± 1.0%). This phenomenon likely relates to the accumulation of mitotic cells along the ventricle, as observed in the histopathological analysis (Figs. 1A-c and B). At 9 h, the number of cells in G2/M further increased (16.1 ± 0.6%), that of S phase increased slightly, and that of G0/G1 decreased. These results suggest that cell cycle progression was blocked and delayed at the S/G2 and G2/M transitions. Although phospho-histone-H3-positive cells with mitotic figures decreased at 9 h compared to 6 h (Fig. 1B), the number of cells in the G2/M phase increased at 9 h. It indicates that, at 9 h, G2 progression was blocked while the degree of mitotic accumulation decreased. Furthermore, apoptotic cells began to appear in the sub-G1 area from 6 to 9 h after 5AzC treatment. At 12 h, the number of cells accumulated in G2/M was reduced, the number of cells in the S phase decreased, and that of G0/G1 increased. At the same time, the number of apoptotic cells remarkably increased (15.8 ± 3.2%). In light of these results, the G2/M block appeared to have been released and the cells shifted to G0/G1 after mitosis, or to apoptosis.

Detection of BrdU-positive cells in the cell cycle

To confirm that cells shifted from accumulation at G2/M and either entered G0/G1 or became apoptotic, we injected BrdU (20 mg/kg) and used a flow cytometry to investigate the cell cycle transition of 5AzC-treated neural progenitor cells. 5AzC and BrdU both are incorporated into DNA during the S phase of the cell cycle.

In the BrdU-only control group, BrdU first was incorporated into S-phase cells at 1 h after treatment (Fig. 3). At 3 h, the BrdU-incorporated cells had transitioned from S to G2/M phase, and some had entered G0/G1. At 6 h, most of the BrdU-positive cells had exited S phase and were in G2/M or G0/G1. At 9 h, some BrdU-positive cells had re-entered S phase, and most of them had returned to S phase by 12 h. The duration of a single complete cell cycle is thought to be at least 12 h, an assumption that is supported by the previous reports (von Waechter and Jaensch, 1972; Takahashi et al., 1995).

When 5AzC was injected with BrdU, BrdU-incorporated cells transitioned from S to G2/M phase during hours 1 through 3. At 6 h, more 5AzC-treated cells than control cells were still in G2/M (control, 16.5 ± 3.4%; 5AzC, 43.6 ± 6.7%). Many of these cells likely were in M phase because most of the abnormal mitotic cells were BrdU-positive in our previous study (Ueno et al., 2002a). At 9 h, most of them still remained in the G2/M phase (control, 5.3 ± 1.9%; 5AzC, 23.9 ± 2.7%), but some cells had moved to G0/G1. In our previous results, at 9 h, small number of BrdU-positive cells (about 4%) were mitotic cells

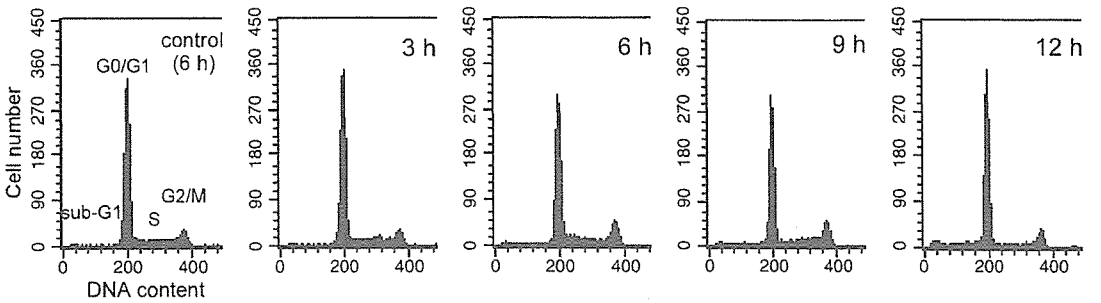

	control (6 h)	3 h	6 h	9 h	12 h
Sub-G1	0.6 ± 0.3 (%)	0.5 ± 0.1	5.0 ± 1.2*	7.0 ± 1.7*	15.8 ± 3.2*
G0/G1	72.5 ± 1.4	71.6 ± 0.2	61.6 ± 1.0*	56.6 ± 3.0*	63.2 ± 3.2*
S	18.1 ± 0.7	19.0 ± 0.8	18.3 ± 1.0	20.3 ± 1.7	10.8 ± 0.9*
G2/M	8.8 ± 0.7	8.9 ± 0.9	15.0 ± 0.9*	16.1 ± 0.6*	10.2 ± 0.3*

Fig. 2. Cell cycle analysis of telencephalic cells in the rat fetus (*x* axis: PI intensity (DNA content), *y* axis: cell number). Percentages for each cell cycle phase are presented as the mean ± SD of 3 dams. The treatment of 5AzC increased the number of G2/M cells from 6 to 9 h and apoptotic cells in the sub-G1 area from 6 to 12 h. *$P < 0.05$; significantly different from the control (6 h) (Student's *t* test).

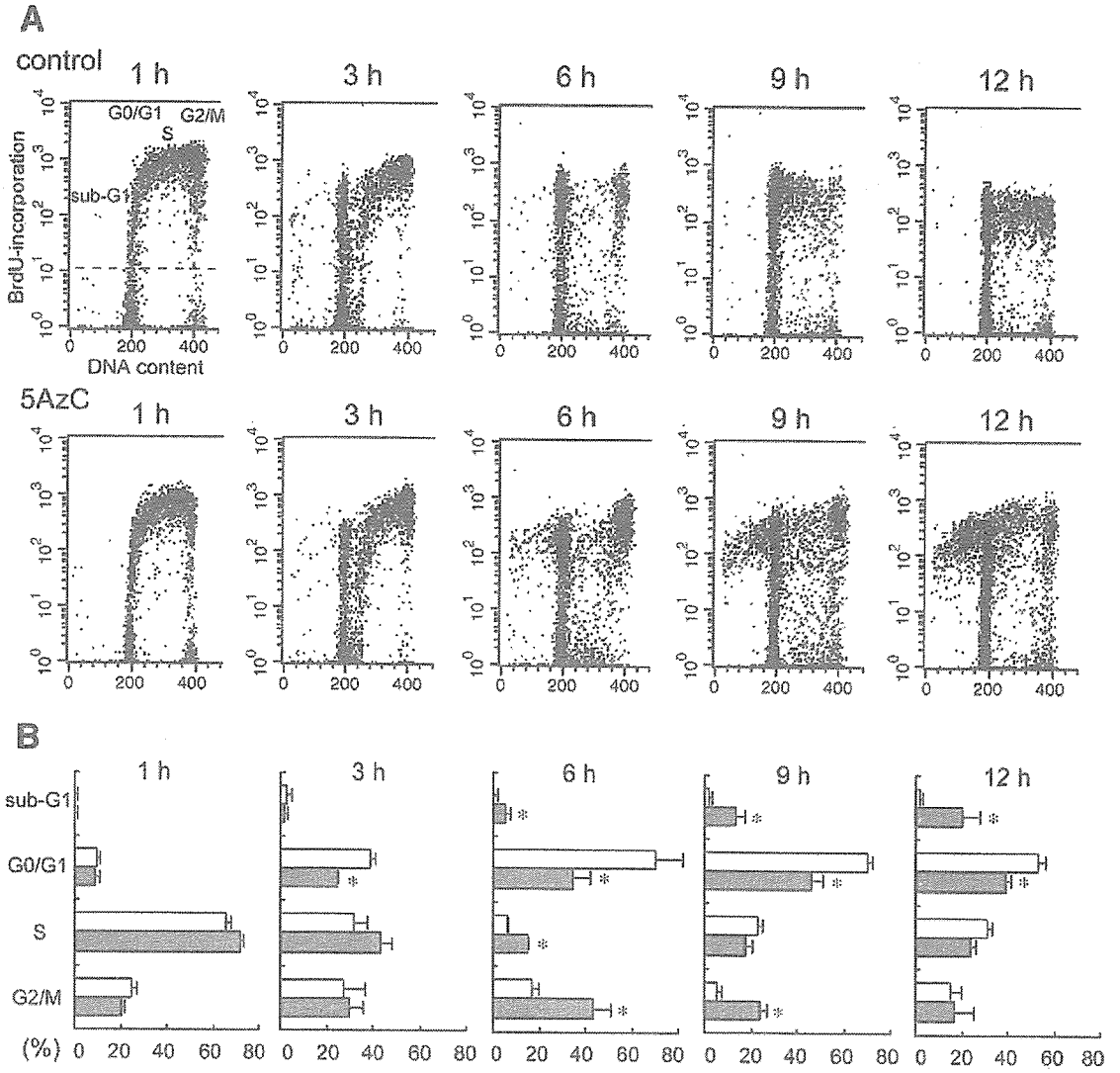

Fig. 3. Transition of BrdU-incorporated telencephalic cells of rat fetus in the cell cycle. (A) Detection of BrdU-incorporated cells in the cell cycle using flow cytometry (*x* axis: PI intensity (DNA content), *y* axis: FITC intensity (BrdU incorporation)). The cells that have FITC intensity above the dotted line are BrdU-positive cells. (B) Distribution of BrdU-positive cells in the cell cycle (white bar: control group, gray bar: 5AzC-treated group). Percentages for each cell cycle phase are presented as the mean ± SD of 2 dams. $^{*}P < 0.05$; significantly different from the control group (Student's *t* test). By 5AzC treatment, BrdU-positive cells were accumulated in G2/M phase from 6 to 9 h, and then they transited to G0/G1 or sub-G1 area (apoptosis).

(Ueno et al., 2002a), suggesting that G2 progression was inhibited in this period. Furthermore, some BrdU-positive cells had undergone apoptosis, as demonstrated by the increase in the sub-G1 area (13.3 ± 3.3%). At 12 h, the cells moved to G0/G1 or to the sub-G1 area, which contained apoptotic cells. These results indicate that cell cycle progression of 5AzC-treated neural progenitor cells was blocked in M phase at 6 h and in G2 phase at 9 h, after which the cells either entered G0/G1 phase or became apoptotic.

Cell cycle position of cells undergoing apoptosis

We then sought to confirm whether the 5AzC-treated apoptotic cells had died before or after mitosis. The results of our cell cycle analysis were consistent with those of our histopathological examination, showing that apoptotic cells began to increase at 9 h and that the number peaked at 12 h after 5AzC treatment (Ueno et al., 2002a,b, and Fig. 1C). To clarify at which cell cycle phase 5AzC-treated neural progenitor cells undergo cell death, we used flow cytometry to assess the presence of DNA strand breaks in cells versus their DNA content. The cells first were fixed with paraformaldehyde, which prevents apoptotic cells from losing their DNA fragments (loss of DNA fragments causes the cells to stain as a sub-G1 population) (Gorczyca et al., 1993; Murakami et al., 1995). In this way, the apoptotic cells with the DNA contents indicative of G0/G1, S, or G2/M phases can be detected, thus clarifying during which phase the cells died.

The results of the flow cytometric analysis of the paraformaldehyde-fixed cells are shown in Fig. 4. From 9 to

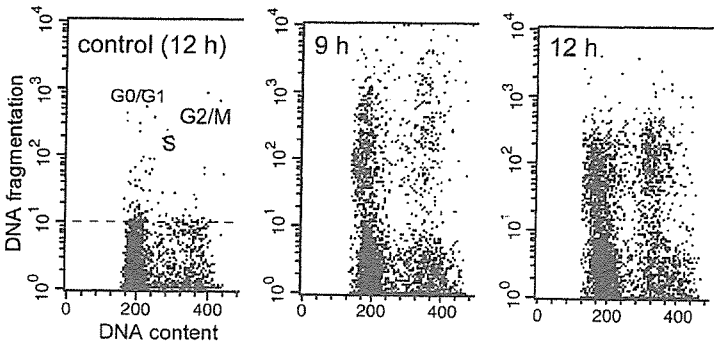

Apoptotic cell	1.8 ± 1.4 (%)	10.5 ± 3.6	19.5 ± 2.1
G0/G1	68.7 ± 5.4	65.0 ± 5.8	56.6 ± 3.7
S	18.4 ± 4.5	9.2 ± 1.5	9.6 ± 1.3
G2/M	12.9 ± 1.1	25.8 ± 4.9	33.8 ± 4.9

Fig. 4. Apoptotic cells and their DNA content in 5AzC-treated rat fetal telencephalon (*x* axis: PI intensity (DNA content), *y* axis: FITC intensity (DNA fragmentation)). The cells that have FITC intensity above the dotted line are BrdU-labeled apoptotic cells. Percentages of apoptotic cells and their cell cycle distribution are presented as the mean ± SD of 3 dams. 5AzC-induced apoptosis mainly occurred in G1, while also in G2/M and S phase.

12 h after the treatment, most of the cells undergoing apoptosis were in G0/G1 phase (9 h, 65.0 ± 5.8%; 12 h, 56.6 ± 3.7%), although some were in G2/M and S phases. At 12 h, the ratio of apoptotic cells in the G0/G1 phase decreased and that in the G2/M phase increased slightly. The current findings suggest that apoptosis predominantly is induced after the mitosis, but some cells die before. These results are consistent with our previous report, which showed that some neural progenitor cells underwent apoptosis after mitosis (Ueno et al., 2002a).

p53 and G2/M checkpoint proteins

In our previous study, we suggested that p53 and its transcriptional target genes play important roles in 5AzC-induced toxicity in the neural progenitor cells (Ueno et al., 2002a). In addition, the present cell cycle analysis further demonstrated that 5AzC inhibited G2/M progression. Therefore, we focused on p53 and cell cycle regulators in G2/M phase and examined the expression of these proteins.

The expression of p53 protein was elevated during hours 6 through 12 (Fig. 5A), a finding consistent with our previous immunostaining results (Ueno et al., 2002a). The expression of $p21^{waf1/cip1}$, a CDK inhibitor and target gene of p53, also increased (Fig. 5A). We therefore examined cell cycle alteration in p53-knockout mice to confirm the influence of p53 on the cell cycle and apoptosis. Histopathological evaluation revealed abnormal accumulation of mitotic cells along the ventricle at 6 h in every p53 genotype (Figs. 5B-a to c), suggesting that mitotic progression was blocked. These mitotic cells were positive for phospho-histone H3 (Figs. 5B-g to i). At 12 h, pyknotic cells positive for cleaved caspase-3 were observed in the $p53^{+/+}$ (wild-type) and $p53^{+/-}$ mice, but not in the $p53^{-/-}$ mice (Figs. 5B-d to f and j to l). In the cell cycle analysis (Fig. 5C), the number of G2/M cells increased in every genotype at 6 to 12 h (6 h; +/+, 15.7 ± 1.0%; +/−, 14.4 ± 1.9%; −/−, 14.2 ± 0.7%, 12 h; +/+, 13.8 ± 3.0%; +/−, 16.9 ± 3.4%; −/−, 19.1 ± 2.9%). The number of mitotic cells decreased in every p53 genotype at 12 h (Figs. 5B-d to f) compared to that at 6 h (Figs. 5B-a to c), while the number of G2/M cells increased at 12 h, suggesting that G2 progression was blocked at 12 h. At 12 h, the number of apoptotic cells in the sub-G1 area increased only in the $p53^{+/+}$ and $p53^{+/-}$ mice (+/+, 21.2 ± 6.3%; +/−: 11.2 ± 3.1%; −/−, 2.8 ± 1.5%). $p53^{-/-}$ neural progenitor cells escaped from apoptosis at 12 h, although the number of cells in the G2/M phase increased through the 6- and 12-h time points. These results suggest that 5AzC-induced apoptosis is p53-dependent and that the associated M and G2 block are p53-independent. Although S phase accumulation also occurred at 6 to 12 h in the $p53^{+/+}$ animals (Fig. 5C; 6 h, 16.8 ± 3.1%; 12 h, 13.2 ± 2.2%), it occurred only at 6 h in the $p53^{-/-}$ mice (Fig. 5C; 6 h, 15.2 ± 0.8%; 12 h, 6.4 ± 1.8%). Therefore, p53 may play a role in maintaining the inhibition of S-phase progression.

We then undertook DNA microarray analysis to seek the key factors in the regulation of cell cycle. According to the criteria described in Materials and methods, 249 genes were extracted. The expression of some target genes of p53 ($p21^{waf1/cip1}$, *cyclin G1*, *Igfbp3*, *Mdm2*, *Snk*) was upregulated from 6 to 12 h (Table 1). In addition, the expression of some genes involved in the cell cycle regulation was also changed from 6 to 12 h (Table 1).

In the pathway analysis, we noted enhanced expression (mainly at 12 h) of two genes regulating the G2/M transition (*cyclin B1* and *Cdc20*) (Fig. 6A). We confirmed the increased mRNA expression of these genes by using real-time PCR (Fig. 6B). In light of the results in the $p53^{-/-}$ fetal brain and elevated mRNA expression of the genes regulating the G2/M transition, we focused on the p53-independent cascade regulating G2/M transition, and we used Western blotting to examine the expression of cyclin B1, Cdc2 (Cdk1), phospho-Cdc2 (Tyr16), and Chk2 protein (Fig. 6C). Expression of cyclin B1 increased from hours 3 to 9. The amount of phosphorylated Cdc2 was lowest at 6 h and gradually increased from 9 to 12 h, whereas the expression of Cdc2 was nearly unchanged throughout the

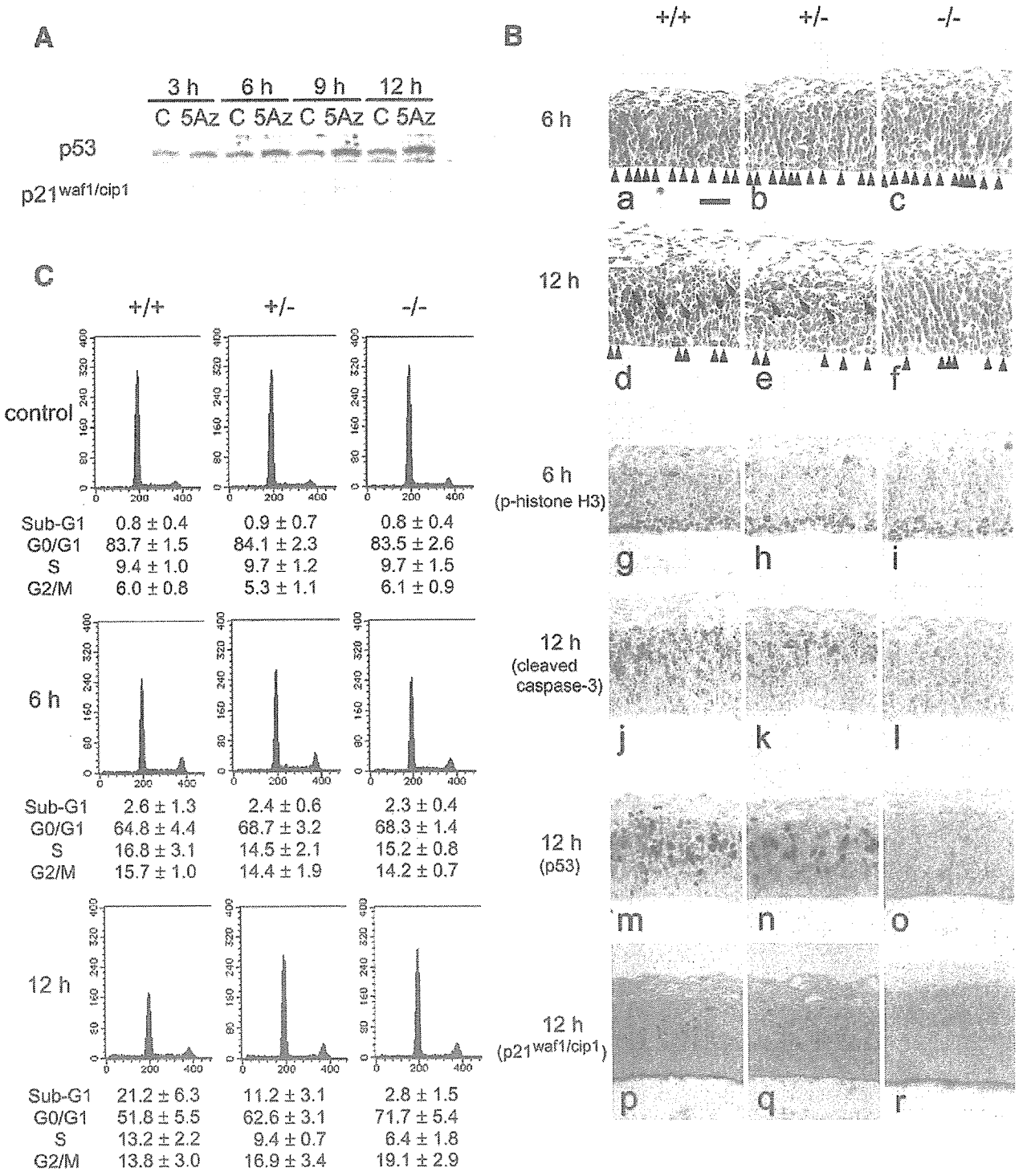

Fig. 5. 5AzC-induced p53-dependent apoptosis and p53-independent G2/M arrest. (A) Western blot analysis of p53 and $p21^{waf1/cip1}$ in control (C) and 5AzC-treated (5Az) rat fetal telencephalon. The expression of p53 and its target gene, $p21^{waf1/cip1}$, increased from 6 to 12 h. (B) Histopathological changes in the VZ of dorsal telencephalic wall of p53-knockout mice fetus. (a–f) Hematoxylin and eosin staining. (g–i) Phospho-histone H3 at 6 h. (j–l) Cleaved caspase-3 at 12 h. (m–o) p53 staining at 12 h. (p–r) $p21^{waf1/cip1}$ staining at 12 h. Accumulation of mitotic cells is observed in every p53 genotype (a–c and g–i, arrowheads: mitotic cells) and then decreased at 12 h (d–f, arrowheads: mitotic cells). Apoptosis is induced in $p53^{+/+}$ and $p53^{+/-}$ mice, but not in $p53^{-/-}$ mice (d–f and j–l, arrows: apoptotic cells). p53 and $p21^{waf1/cip1}$ are expressed in $p53^{+/+}$ and $p53^{+/-}$ mice, but not in $p53^{-/-}$ mice (m–o and p–r). Scale bar: 50 μm. (C) Cell cycle analysis of telencephalic cells of p53-knockout mice fetuses (*x* axis: PI intensity (DNA content), *y* axis: cell number). Percentages for each cell cycle phase are presented as the mean ± SD of 3 dams. In $p53^{+/+}$ and $p53^{+/-}$ mice, the number of G2/M phase cells increased at 6 h and apoptosis in the sub-G1 area at 12 h. In $p53^{-/-}$ mice, the number of G2/M phase cells increased from 6 to 12 h, but apoptosis did not occur remarkably.

Table 1
Expression changes of cell-cycle-related genes in the rat fetal telencephalon treated with 5AzC

Accession no.	Genes	Fold change		
		6 h	9 h	12 h
Cell cycle				
NM_022183.1	topoisomerase (DNA) II alpha (Top2a)		1.33 ± 0.09	
U05341.1	Cdc20/p55CDC			1.52 ± 0.09
X64589.1	cyclin B (Ccnb1)			1.40 ± 0.16
NM_012760.1	lost on transformation 1 (Lot1)/pleiomorphic adenoma gene-like 1 (Plagl1)/Zac1	−1.17 ± 0.05		
NM_054008.1	rgc32 protein (Rgc32)			−1.98 ± 0.47
NM_022683.1	vasopressin-activated calcium-mobilizing receptor protein (VACM-1)/cullin-5 (Cul5)			−1.77 ± 0.72
NM_021662.1	DNA polymerase delta, catalytic subunit (Pold1)			−1.52 ± 0.17
NM_017258.1	B-cell translocation gene 1, anti-proliferative (Btg1)			−1.37 ± 0.2
p53-target genes				
NM_012923.1	cyclin G1 (Ccng1)	1.93 ± 0.00	3.02 ± 0.38	3.23 ± 0.03
U24174.1	p21 (Waf1/Cip1)		4.10 ± 2.77	
BF548539	ESTs, Moderately similar to S15349 mdm2 protein-mouse (*M. musculus*)		1.63 ± 0.04	
NM_031821.1	serum-inducible kinase (Snk)/Plk2		1.42 ± 0.19	
NM_012588.1	insulin-like growth factor-binding protein (Igfbp3)		2.30 ± 0.98	1.86 ± 0.32

Fold change is presented as the mean ± SD of 2 arrays.

experimental period. The expression and mobility of Chk2 protein did not change through the experimental period.

Discussion

We showed that neural progenitor cells underwent G2/M accumulation and apoptosis due to 5AzC-induced stresses in the fetal CNS. Apoptosis likely is induced by a p53-dependent mechanism, and G2/M block probably occurs in a p53-independent manner.

5AzC is a cytidine analogue and has a DNA demethylating effect on cells. Incorporation of 5AzC into the CpG island of the DNA promoter region leads to exchange of deoxycytidine for 5AzC, and this exchange blocks DNA methylation. As mentioned before, in the developing brain, DNA methylation is a key step for regulating gene expression (Sun et al., 2003). Therefore, 5AzC may disturb gene expression and alter organogenesis through its DNA demethylating effect. In our DNA microarray analysis, it failed to identify any gene whose expression was upregulated by the demethylating effect, although only a few genes currently are known to transcriptionally regulate by DNA methylation in the developing brain. For example, the astroglial markers GFAP and S100β are hypermethylated in the early to mid developing brain before glial cells are produced (Sun et al., 2003; Takizawa et al., 2001; Namihira et al., 2004); however, their expression was unchanged at 6 to 12 h after 5AzC treatment (data not shown). Therefore, we were unable to definitively determine the role of 5AzC-induced demethylation in neural progenitor cells of the developing brain.

5AzC also acts as a DNA-damaging agent. When 5AzC or 5-aza-2′-deoxycytidine, which has deoxyribose instead of the ribose of 5AzC, is incorporated into DNA, it forms a covalent bond with DNA methyltransferase (Santi et al., 1984; Michalowsky and Jones, 1987; Ferguson et al., 1997), resulting in DNA damage (Juttermann et al., 1994; Karpf et al., 2001). Indeed, elevated expression of p53, known as a 'guardian of the genome', has been documented to occur after 5AzC or 5-aza-2′-deoxycytidine treatment (Karpf et al., 2001; Zhu et al., 2004). p53 plays a key role in DNA repair, cell cycle arrest, and apoptosis in response to DNA damage caused by irradiation, chemical treatments, and so on (May and May, 1999).

In our previous and present studies, we confirmed that p53 expression was augmented at the protein level in neural progenitor cells (Ueno et al., 2002a, and Figs. 5A, B-m) and that the expression of some target genes of p53 (*p21$^{waf1/cip1}$*, *cyclin G1*, *Igfbp3*, *Mdm2*, and *Snk*) was upregulated (Ueno et al., 2002a and Table 1). We therefore surmise that 5AzC exerts a toxic effect via DNA damage. However, in some contexts, such as loss of DNA methyltransferase, disturbance of the methylation state of the DNA from its normal pattern causes elevated p53 expression and cell death (Jackson-Grusby et al., 2001). Therefore, we cannot exclude the possibility that the toxicity of 5AzC is associated with a DNA demethylating effect.

We have shown that 5AzC induces a p53-dependent apoptosis (Figs. 5B and C), although the mechanism by which 5AzC activates p53 remains obscure. In contrast, the 5AzC-associated G2/M accumulation seems to be p53-independent. In the microarray and signal pathway analyses, the expression of genes that promote G2/M transition (*cyclin B1* and *Cdc20*) was upregulated (Figs. 6A and B), so we investigated an alternative pathway of cell cycle regulation. For the G2 to M transition, the activation of Cdc2 kinase (Cdk1) and its interaction with cyclin B1 are indispensable. Chk1 and Chk2 are serine kinases, which